NULL GEODESIC DEVIATION EQUATION AND MODELS OF GRAVITATIONAL LENSING

by

Krishna Mukherjee

B.Sc. (Hons.), Calcutta University, 1977

M.Sc., Calcutta University, 1980

M.S., University of Kansas, 1989

M.S., University of Pittsburgh, 1999

Doctor of Philosophy

Submitted to the Graduate Faculty of

Arts and Sciences in partial fulfillment

of the requirements for the degree of

Doctor of Philosophy

University of Pittsburgh

2005

UNIVERSITY OF PITTSBURGH

Arts and Sciences

This dissertation was presented

by

Krishna Mukherjee

It was defended on November 10, 2005

and approved by

Andrew J. Connolly, Associate Professor, Department of Physics & Astronomy

Simonetta Frittelli, Adjunct Associate Professor, Department of Physics & Astronomy

Rainer Johnsen, Professor, Department of Physics & Astronomy

George A. J. Sparling, Associate Professor, Department of Mathematics

Co-Advisor: Ezra T. Newman, Professor Emeritus, Department of Physics & Astronomy

Co-Advisor: David A. Turnshek, Professor, Department of Physics & Astronomy

NULL GEODESIC DEVIATION EQUATION AND MODELS OF GRAVITATIONAL LENSING

Krishna Mukherjee, Ph.D.

University of Pittsburgh, 2005

A procedure, for application in gravitational lensing using the geodesic deviation equation, is developed and used to determine the magnification of a source when the lens or deflector is modeled by a "thick" Weyl and "thick" Ricci tensor. This is referred to as the Thick Lens Model. These results are then compared with the, almost universally used, Thin Lens Model of the same deflector. We restrict ourselves to spherically symmetric lenses or, in the case of a thin lens, the projection of a spherically symmetric thin lens into the lens plane. Considering null rays that travel backward from the observer to the source, the null geodesic deviation equation is applied to neighboring rays as they pass through a region of space-time curvature in the vicinity of a lens. The thick lens model determines the magnification of a source for both transparent and opaque lenses. The null rays passing outside either the transparent or opaque lens are affected by the vacuum space-time curvature described by a Schwarzschild metric and transmitted via a component of the Weyl tensor with a finite extent. Rays passing through the transparent lens encounter the mass density of the lens, chosen to be uniform. Its influence on the null geodesics is determined by both the Weyl and Ricci tensor with the use of the Einstein equations. The curvature in the matter region is modeled by a constant Weyl and constant Ricci tensor. We apply the thick lens model to several theoretical cases. For most rays outside the matter region, the thick lens model shows no significant difference in magnification from that of the thin lens model; however large differences often appear for rays near the Einstein radius, both in the magnification and in the size of the Einstein radius. A small but potentially measurable discrepancy between the models arises in microlensing of a star. Larger discrepancies are found for rays traversing the interior of a transparent lens. This case could be used to model a galactic cluster.

TABLE OF CONTENTS

LIST OF FIGURES

PREFACE

There are many people I would like to thank for their help with the work presented here. I owe a profound gratitude to my advisor Ezra T. Newman. At every step of this dissertation he guided me and has taught me not just to think but also to write like a physicist. I am extremely grateful to my co-advisor David A. Turnshek who showed me how to think and analyze data like an astronomer. I owe a deep gratitude to Simonetta Frittelli who helped me to understand the mathematical approximations that are necessary in a theoretical model. To Andrew Connolly I am grateful for the conversations I have had with him regarding the applications of my model to cosmology. I am grateful to Rainer Johnsen who guided me throughout my graduate career and to George Sparling for his comments on my dissertation. I would also like to thank Allen Janis for his many valuable comments which have improved my work. I am grateful to David Jasnow for giving me adequate time to finish this dissertation and in believing in me. I would also like to thank Leyla Hirschfeld for her help with all the paper work. I am grateful to all my colleagues at Slippery Rock University for their continuous support.

Finally I would like to thank my family, my parents Aruna and Ashis Chakravarty, my husband Pracheta and specially my mother-in-law, the late Gouri Mukherjee without whose constant encouragement this dissertation would never have been completed.

1.0 BRIEF HISTORY OF GRAVITATIONAL LENSING

The effect of the gravitational field of a massive object on light rays has been studied by many in the last 300 years. That massive bodies could have this effect was first suggested by Isaac Newton in 1704. According to Newtonian theory the bending of the light rays is inversely proportional to the impact parameter and directly proportional to the deflecting mass. When the deflecting object's density is sufficiently large, Mitchell (1783) and Laplace (1786) showed that the deflection angle is so extreme that light can be trapped or self generated light never escapes from the massive body. Such objects are now recognized as black holes. In 1801, J. Soldner published a paper that calculated for the first time the deflection angle of a light ray at grazing incidence to the surface of the sun. Using Newtonian mechanics Soldner derived a value of 0.84 arc seconds for this angle. A century later, with his newly discovered theory of general relativity, Albert Einstein (1911, 1915) obtained a value twice that of Soldner's. Einstein's prediction was verified when Eddington and Dyson observed the deflection angle within the range of permissible error during the solar eclipse of 1919.

Little did physicists and astronomers realize then that observation of light deflection by cosmic bodies would open an entirely new research field now referred to as "gravitational lensing" which both validates general relativity and becomes a tool for the study of astronomical and cosmological phenomena.

1.1 TYPES OF GRAVITATIONAL LENSING

A gravitational lens system (here after abbreviated as GL) is comprised of a light source, an intervening matter distribution that acts as the gravitational lens and an observer who sees images of the source. The simplest example of such a system would be the perfect alignment of the observer with a spherical lens and source. It produces a magnified image of the source in the form of a ring, known as the Einstein ring. Other configurations of GL system's can lead to multiple images. Both Chwolson (1924) and Einstein (1936) were skeptical of the Einstein ring or double images ever being observed because of the small angular radius of the ring and the arc second separation of images. It was Fritz Zwicky (1937) who envisioned the potential for observing separate images of sources that are lensed by large masses, as for example, galaxies instead of stellar masses.

In the sixties Refsdal (1964; 1966) wrote several important papers working out the details of gravitational lensing; in one he demonstrated that quasars as sources could be used to determine the mass of lensing galaxies from the angular separation of their images and in the other he explained how variability in a quasars' intrinsic brightness could be used to constrain one of the cosmological parameters, the Hubble constant. If the lensing system was asymmetrical, light rays could follow different path lengths to the observer who could measure a time delay by the flux variations between the pair of images. From the time delay and combining it with the redshift information of the images, Refsdal showed that the Hubble constant could be calculated (figure 1.1).

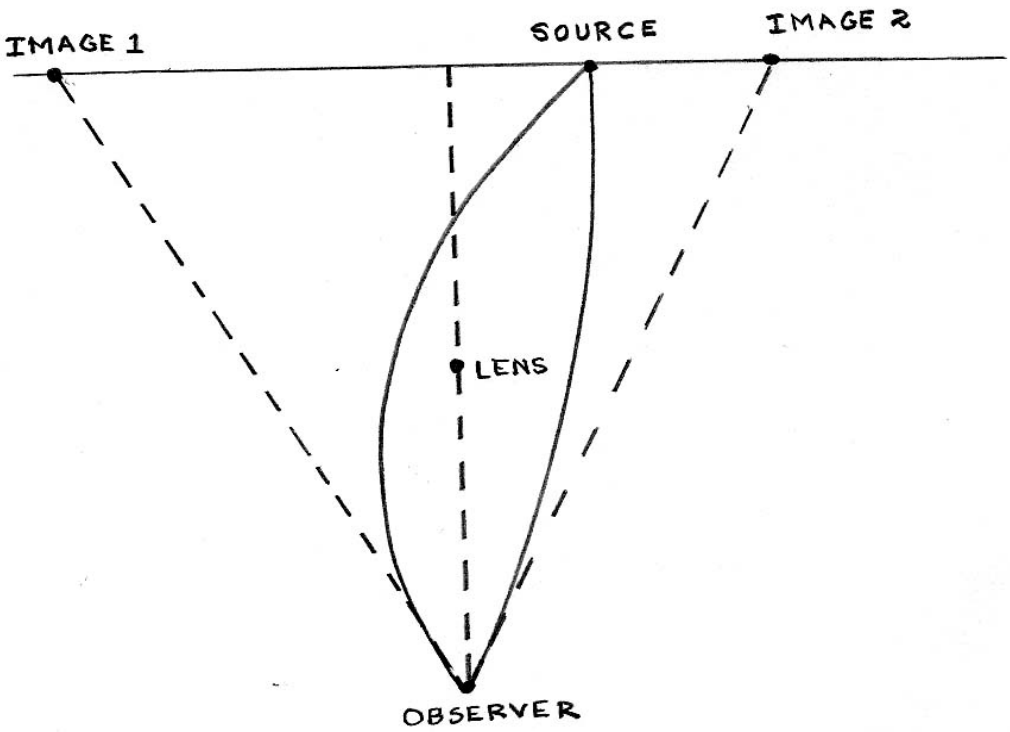

Figure 1.1 Deflection of light rays from a source due to a gravitational lens

With the discovery of the first gravitational lensed quasar by Walsh et al. (1979) the age of observational lensing was launched. Observational studies of gravitational lensing have now branched off into two categories. Lenses that create multiple images and have large magnification belong to the group called strong lenses; those that have large impact parameters produce a single image with some distortion in the image and small magnification of the source fall under the category of weak lenses. Besides strong and weak lensing, in the late seventies and eighties another area in gravitational lensing, called "microlensing" was explored by astronomers. Microlensing is the gravitational lensing of a source by another star or an object

smaller than a star. Chang and Refsdal (1979) showed that image separations of a micro arc second were not discernible; however the relative motion between the source and a micro-lensing star, which would change their alignment, results in variable image magnification which is observable.

We now discuss several examples from these three areas of gravitational lensing.

1.1.1 Strong Lensing

The images of a gravitationally lensed quasar in the shape of a cross (four images) was discovered by Huchra (1984). These were later referred to as the Einstein cross. Other Einstein crosses have since been discovered with one particular cross observed by Rhoads et al. (1999) located within the bulge of the galaxy. The first Einstein ring with an angular diameter of 1.75 arc seconds was imaged by Hewitt et al. (1988) using the Very Large Array radio telescope. Today many GL systems show multiple images of quasars while a few also show Einstein rings. Often a partial ring is observed; Cabanac et al. (2005) has found a 270 degree ringed image with an angular diameter of 3.36 arc seconds.

1.1.2 Weak Lensing

The first giant arcs that were distorted images of distant galaxies were observed around a galaxy cluster by Soucail et al. (1986) and Lynds et al. (1986). Faint images of background galaxies oriented tangentially around galaxy clusters were first recognized by Tyson et al. (1990) as weak lensing signals. These signals were later used by Kayser and Squires (1993) to determine the

surface mass distribution of the cluster. Arcs provide valuable information about the existence and the quantity of the dark matter content in clusters.

Researchers like Jaroszynski et al. (1990), are studying how weak lensing can be used to investigate the large scale structure of the universe. Weak GL gives rise to temperature and polarization fluctuations in the cosmic microwave background radiation that can be used to constrain cosmological parameters like the cosmological constant and the critical density of the universe (Metcalf and Silk, 1998). The Sloan Digital Sky Survey researchers, Scranton et al. (2005) did a statistical analysis on the magnification of images of 200,000 quasars as their light rays traveled through dark and visible matter and obtained a lensing signature that confirmed the existence of a non-vanishing cosmological constant and overwhelming abundance of dark matter over visible matter in our universe. Today galactic clusters act as huge cosmic lenses that reveal distant galaxies in the form of multiple tangential arcs or in the form of a single distorted image. This allows astronomers to find the red shift distribution of faint galaxies. By analyzing the spectral lines of the arcs, the star formation rate and morphology of these distant galaxies can be determined (Mellier, 1999).

1.1.3 Microlensing

By monitoring the light curves of stars in the Large Magellanic Cloud, Paczynski (1986) predicted that it would be possible to detect massive compact halo objects (MACHO) having masses in the range of one tenth to one hundredth of the solar mass in our galaxy acting as "micro" lenses. This opened up a whole new era in microlensing research. In the last decade there has been a concerted effort by many groups of astrophysicists (OGLE, "Optical Gravitational Lensing Experiment", EROS, "Experience pour la Recherche d'Objets Sombres"

and MACHO) to detect microlensing events by observing millions of stars in the Large Magellanic Cloud that are lensed by our Galaxy's halo members. Quasar microlensing by Wambgnass et al. (2002) has recently shown potential for determining the sizes of emitting regions in quasars.

Recently several observer groups (MPS, Microlensing Planet Search, PLANET, Probing Lensing Anomaly Network, MOA, Microlensing Observations in Astrophysics) have focused their attention on microlensing events to detect extrasolar planets. Discovery of the first extrasolar planet by gravitational lensing by Udalski et al. (2005) was possible when a microlensed star showed sharp increase in magnification in its light curve. The spikes in the light curve were due to lensing by the orbiting planet and from the duration of such an event the size of the planet could be estimated. Similarly detailed analysis of light curves of microlensing events by Rattenbury et al. (2005) have led to the determination of the oblate shape of a star due to its rotation.

1.1.4 Flux variation in strong, weak and microlensing GL system

Observation of some gravitational lens systems with radio telescopes and the Hubble Space Telescope have revealed anomalous flux ratio of images (Xanthopoulos, 2004; Jackson et al., 2000; Turnshek et al. 1997). The anomalies refer to the different ratios obtained from theoretical analysis and observation. There are a variety of possible causes for these anomalies. They could be due to microlensing caused by stars in the lensing galaxy or in systems where the flux varies with wavelength (Angonin-Willaime et al., 1999). There could be extinction due to inhomogeneous dust distributions in the lensing galaxy. Some have speculated that the variation in image fluxes could be due to the proximity of multiple lenses (Chae and Turnshek, 1997); in

the case of multiple imaged quasars it could be explained by the substructure in the dark matter halos as suggested by Metcalf et al. (2004) or by the varying sizes of the emission regions of the quasars, Moustakas and Metcalf (2005). If it was properly understood, the magnification anomalies could provide considerable insight into the structure of lensing matter, Metcalf and Zhao (2002) and its dark matter content, Mao et al. (2004).

The purpose of the present work was first to examine an alternative method to determine the magnification of the source in a GL system that differed from that of the standard thin lens approximation and second, to see if this approach could address some of the observed magnification anomalies. This alternative method was based on using a thick lens rather than the usual thin lens approximation.

1.2 THIN LENS APPROXIMATION

The thin lens approximation arises from the fact that the light deflection from a light source takes place near the lens over a spatial length that is extremely small compared to the total light path. Observationally this is true for most gravitational lens system since the distances involved are enormous compared to the dimension of the lens. This becomes the justification for replacing the three dimensional mass distribution of a lens by a two dimensional sheet of mass defining the lens plane and is also the rationale for using the term “thin lens”.

The derivation of the thin lens equation, which relates via the astronomical parameters, the apparent source position in the sky due to the deflection to that of the un-deflected position, is given in chapter 2.

1.3 DEFINITION OF A THICK LENS

To describe the thick lens and the thick lens approximation that we will be using, we consider an extended space-time source whose world tube intersects the past light cone of an observer (Figure 1.3.1). The cross-section of the light cone at the intersection of the source's world tube determines the source's visible shape. The pencil of null rays that join this cross-section to the observer transfers the information regarding the source's shape to the observer.

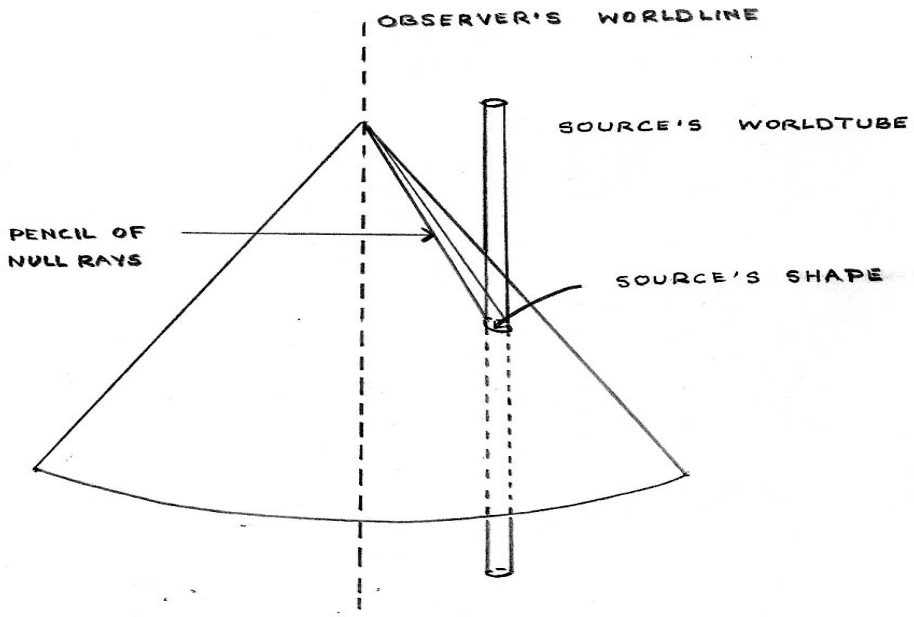

Figure 1.3.1 Observer's past light cone

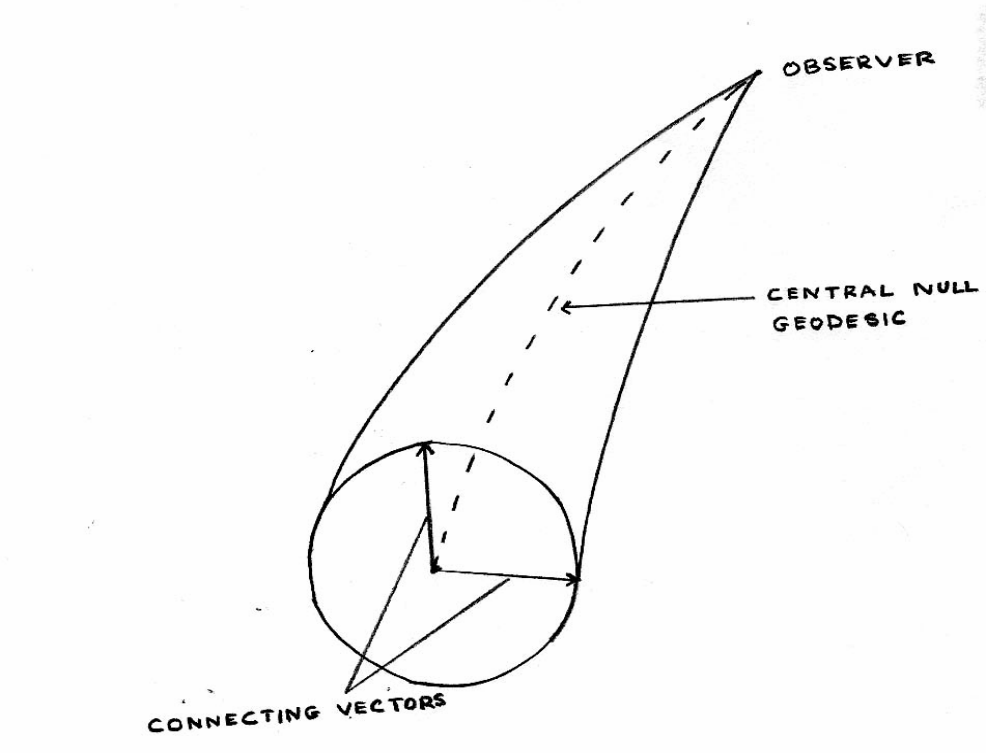

Figure 1.3.2 Intersection of source's worldtube with observer's past light cone

An extended source is a collection of individual points; each of these points is mapped onto the observer's celestial sphere via individual null geodesics to form an image of the source. By assuming a small source, we can focus on a single null geodesic, the one that connects the center of the source's cross-section to the observer, and describe the relationship between the source's shape and the image's shape by "connecting vectors" along the central null geodesic (Figure 1.3.2). These connecting vectors or Jacobi fields satisfy the geodesic deviation equation along the central null geodesic and connect the latter to neighboring null geodesics belonging to the pencil of null rays (Frittelli, Kling & Newman, 2000)

Far from the lens and near the source, we assume a flat space-time, but closer to the lens the space-time curvature has a non-trivial effect on the deviation vector. Astrophysical lenses have a mass distribution over a finite region. Granted the spatial dimension is small compared to the distances involved, nevertheless in this thesis we want to study whether the finite extent of this region's curvature could affect the null geodesic deviation vectors and thereby change the magnification of the source significantly from the magnification obtained by the thin lens approximation.

We choose spherically symmetric lenses that are described by a Schwarzschild metric outside the matter distribution of the lens. The geodesic deviation equation involves two tensors, the Ricci and the Weyl as sources. Both the Ricci tensor, which is a measure of the mass density of the lens, and the Weyl tensor describe the gravitational field inside the matter region of the lens while in the neighboring vacuum region of space-time outside only the Weyl tensor is of relevance.

Our definition of a “thick lens” is an approximation consisting of a finite region where we assume a constant Weyl curvature and a smaller region of uniform mass density (Figure 1.3.3) or constant Ricci tensor.

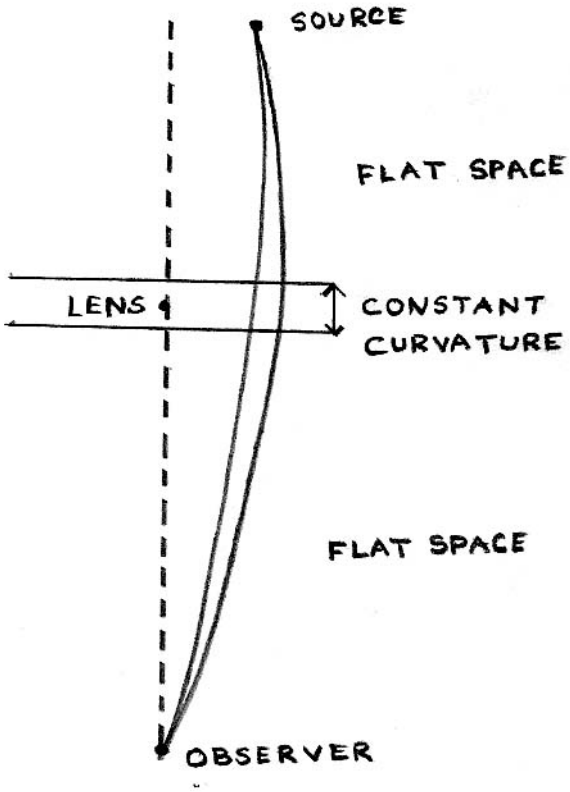

Figure 1.3.3 Illustration of region of constant curvature

Our model which we shall describe in detail in chapter 3, is illustrated in Figure 1.3.4. We choose null geodesics from the source to the observer that passes through a region of the constant Weyl tensor and, depending on the size of the impact parameter, through the matter

region of constant Ricci tensor of the lens. Part of the approximation is to determine these null geodesics via the thin lens equation. We then seek a solution to the geodesic deviation equation along the entire trajectory of the null geodesic from the observer to the source. The derivation of the magnification of the source from the deviation vectors is described in chapter 3. The basic difference between our derivations of the magnification versus the conventional derivation is that instead of using the lens equation in the thin lens model we use the geodesic deviation vector to compute the magnification. We then compare the magnification obtained from our thick lens model with that of the thin lens model for different lensing masses and sizes. They will be discussed in chapter 4 and 5.

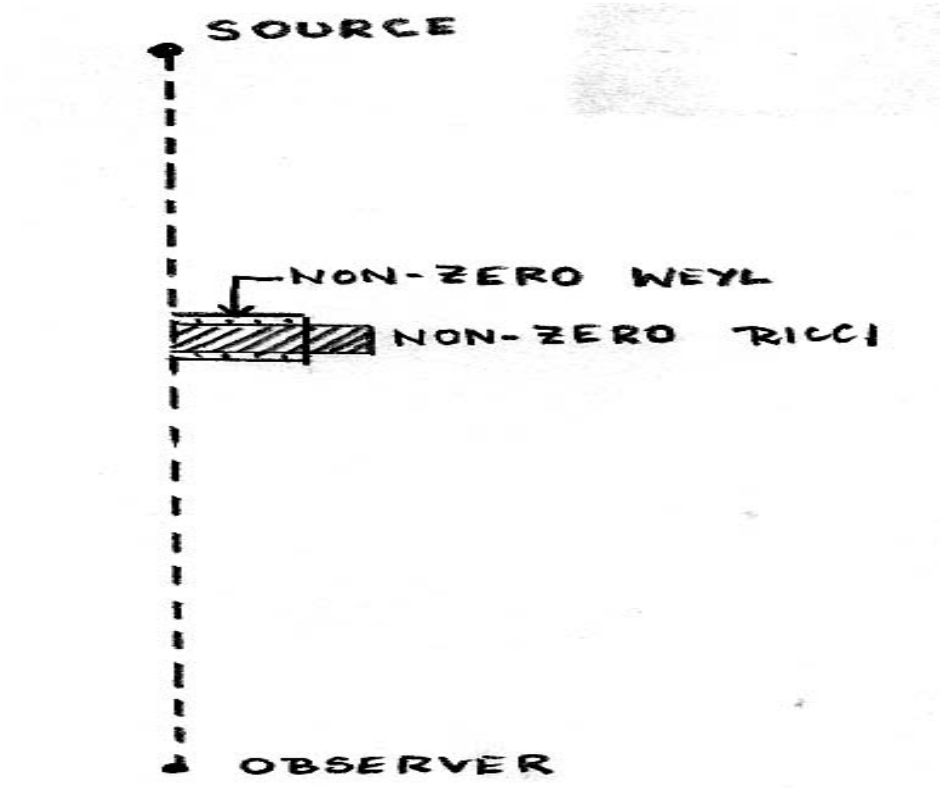

Figure 1.3.4 Thick lens model

1.4 OTHER THICK LENS MODELS

We mention several other attempts at thick lens models. Using Newtonian approximation Bourassa and Kantowski (1975) had studied a transparent lens by projecting a "thick" spheroidal volume mass density (density inversely proportional to the semi-major axis) on to the lens plane, thus essentially working in the thin lens approximations.

Hammer (1984) examined a thick lens model similar to the one developed here to compute the amplification of the light source. He chose the background to be a low density Friedmann solution with a vacuum Schwarzschild region near the lens and the matter density of the lens as high density Friedmann solution. From the optical scalar equation he obtains the ratios of the light beam diameters with and without the lens as a power series expansion as a product of the lens radius and the Hubble constant scaled by the velocity of light. This work in point of view is closest to ours. The thick lens calculations are done in a cosmological background with no use of Schwarzschild Weyl tensor.

Kovner (1987) had considered a thick gravitational lens that is composed of multi-redshifted thin lenses located at varying distances which is not related to our approach.

Bernardeau (1999) determines the amplification matrix of a lensed source by including cosmological parameters in the optical scalar equations. This work is similar to Hammer.

Frittelli et al. (1998, 1999), and Frittelli, Kling and Newman (2000) introduced the idealized exact lens map which, in principle, maps by means of the past null geodesics, the observer's celestial sphere, through arbitrary lenses, to arbitrary source planes that contain the light sources. To implement the basic procedure a perturbation theory off Minkowski space had to be developed to find the approximate null geodesics from which the lens equation could be determined. Our work is in some sense an application of this method.

1.5. OBJECTIVE OF THIS WORK AND SUMMARY OF FINDINGS

Rijkhorst has voiced concern (2002) about using the thin lens approximation when an entire galactic cluster acts as a lens. These enormous lenses can be the most stringent test of the thin lens approximation. Thus it may be that the thin lens is not the ideal model to consider in all situations. The other motivation behind this work is to study transparent lenses. Given the observational evidence of Einstein cross located within the bulge of a galaxy and the substructure that astronomers are suspecting within the lens, it seems a study of transparent thick lens model is of possible use. Our goal is to (a) find out whether there is a significant difference in the magnification of the images as calculated from the thin lens and our "thick" lens model. Is the difference sufficiently large so that it could be observed with present or near future telescopes? (b) To see how the magnification of a source is affected by the mass density of a transparent

lens. (c) Does the thick lens approximation predict the same values for the Einstein radius as does the thin lens

We find that, most often, the thick lens magnification did not differ significantly from the thin lens magnification; but there were several exceptions where there was a significant affect. This occurred most often when the impact parameter took the ray close to the Einstein radius. The largest difference in the thick and thin lens magnification occurred for a transparent lens when the null geodesics, for particular impact parameters, passed through the lens. The mass density of the transparent lens determines whether multiple images are observable and the location of these images.

Chapter 2 contains a discussion of the thin lens. This is followed by the development of the thick lens model in chapter 3. In chapter 4 we examine four theoretical lenses and the variation in mass density with the magnification and location of images. In Chapter 5 we describe three configurations of lenses with potential astrophysical applications. Finally, in chapter 6, we summarize our results and discuss possible future developments.

2.0 THE THIN LENS

This chapter contains a review of the thin lens equation, the default equation used for the bulk of lensing work. The material in this chapter relies heavily on the discussion given in Schneider, Ehlers and Falco, (1992) and Narayan and Bartelmann, (1998). In section 2.1 we derive the thin lens equation. The magnification of the source in the thin lens approximation is described in section 2.2. In section 2.3, in order to compare, later in this work, the magnification of the source for a thick spherically symmetric transparent lens with that of a transparent thin lens we describe the thin lens calculations for a spherically symmetric lens projected into the thin lens plane, referring to it as the Projected Spherically Symmetric Thin Lens (PSSTL) model. We will denote the thin lens magnification by μ_0 and for the thick lens by μ_T which we shall derive in the next chapter

2.1 THE THIN LENS EQUATION

On the observer's celestial sphere (Figure 2.1.1, 2.1.2) let the angular positions of the unlensed source S and its lensed image I′ be β and θ respectively.

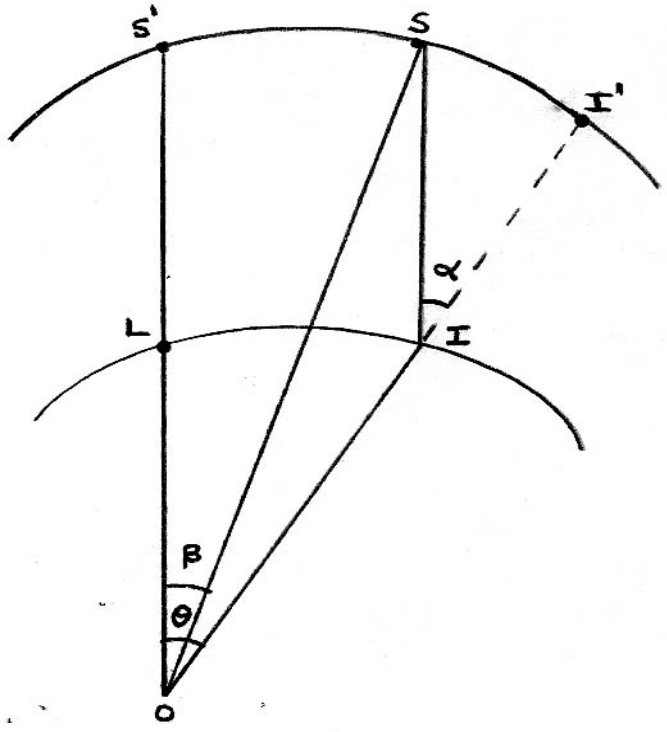

Figure 2.1.1 Angular positions of source and image on the observer's celestial sphere

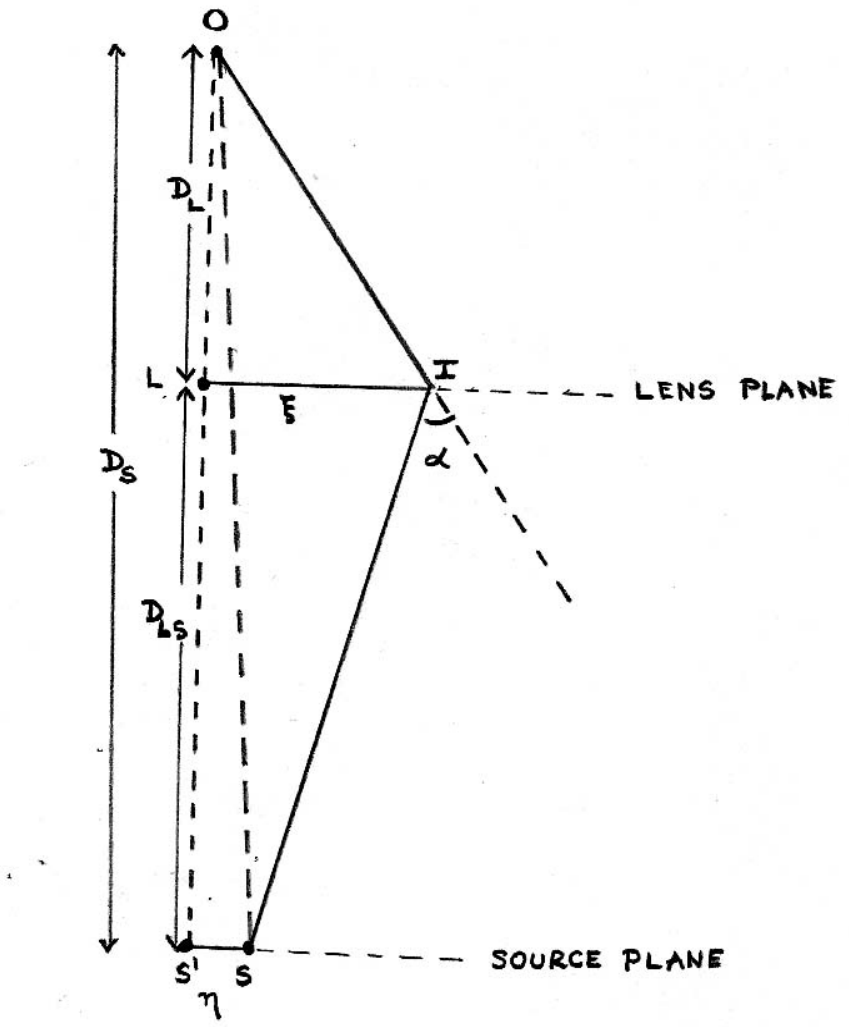

Figure 2.1.2 Model of a thin lens

The line connecting the observer O, with the center of the lens L is known as the optical axis. It is perpendicular to both the lens and source planes and intersects the latter at S′. If D_S is the distance to the source then arc (S′S) = $D_S \sin \beta$ and arc (S′I′) = $D_S \sin \theta$.

In most GL systems the angles β and θ are small, being of the order of a few arc seconds. Using the small angle approximation we have, arc (S′S) = $D_S\beta$ and arc (S′I′) = $D_S\theta$.

A light ray from the source travels in a straight line over flat space. At point I in the lens plane it is bent by an angle α, (the deflection angle), before proceeding to the observer. In the case of the thin lens approximation, the deflection angle is usually considered to be small. Only near a black hole or a neutron star can the deflection angle be extremely large. For example this case was studied by Virbhadra & Ellis (2000). These type of lenses are excluded in the present work.

A relationship between the angular position of the unlensed source and its image can be obtained from the following observation: one can see directly from the lens diagram, figure (2.1.2), the relationship

$$D_S\vec{\beta} = D_S\vec{\theta} - D_{LS}\vec{\alpha}(\vec{\xi}) \qquad (2.1.1)$$

where, $\vec{\beta}$ and $\vec{\theta}$ are the angular vectors describing the location of the source and the image in their respective planes relative to the optical axis and D_{LS} is the distance between the source and the lens. Therefore

$$\vec{\beta} = \vec{\theta} - \frac{D_{LS}}{D_S}\vec{\alpha}(\vec{\xi}) \qquad (2.1.2)$$

which is the thin lens equation used almost universally by the lensing community.

In the special case of a spherically symmetric (Schwarzschild) lens, using linearized Einstein theory, the deflection angle, which becomes a scalar, is given by

$$\alpha = \frac{4GM}{c^2\xi} \qquad (2.1.3)$$

Here, M is the mass of the lens, ξ is the impact parameter of the light ray in the lens plane, G is the universal constant of gravitation and c the speed of light in vacuum.

For a general lens with a given mass distribution in the lens plane, the deflection angle is given by

$$\vec{\alpha}(\vec{\xi}) = \frac{4G}{c^2}\int d^2\xi' \Sigma(\vec{\xi}') \frac{(\vec{\xi} - \vec{\xi}')}{\left|\vec{\xi} - \vec{\xi}'\right|^2} \tag{2.1.4}$$

where Σ is the mass density projected onto the lens plane.

Since we will be considering only spherically symmetric lenses, rotational symmetry permits us to take the observer, lens, source and the optical axis to be coplanar so that equation (2.1.2) can be rewritten as,

$$\eta = \frac{D_S}{D_L}\xi - D_{LS}\alpha(\xi) \tag{2.1.5}$$

where $\eta = D_S \beta$, is the distance of the source from the optical axis in the source plane and $\xi = D_L\theta$, is the impact parameter in the lens plane. D_L is the distance to the lens from the observer. For a spherically symmetric lens, substituting the value of $\alpha(\xi)$ from equation 2.1.3 into the lens equation 2.1.5, we have,

$$\eta = \frac{D_S}{D_L}\xi - \frac{4GM}{c^2\xi}D_{LS} \tag{2.1.6}$$

In the special occasion when the source lies on the optical axis, $\eta = 0$ and $\beta = 0$, then, for a spherically symmetric lens,

$$\alpha(\xi) = \frac{D_S}{D_L D_{LS}}\xi \tag{2.1.7}$$

Substituting equation (2.1.2) into the above, gives

$$\xi = \sqrt{\frac{2GMD_L D_{LS}}{c^2 D_S}} \tag{2.1.8}$$

This particular value of the impact parameter is called the Einstein radius (R_E) and was first calculated by Chwolson (1924) and again by Einstein (1936). Perfect alignment of a GL system gives rise to a luminous ring. The angular radius of the ring, θ_E , which can be measured, is given by,

$$\theta_E = \frac{R_E}{D_L} \tag{2.1.9}$$

Typical observed values of this angle are a few arc seconds. Observational determination of this angle, together with redshift measurement of image and lens distances (Appendix C), provides an estimate of the mass of the lens.

The thin lens equation allows us to calculate the magnification of lensed image of the source. A detail analysis of thin lens magnification is discussed in the next section.

2.2 MAGNIFICATION

The magnification of the source is defined by the ratios of the solid angle subtended by the lensed image and the unlensed image of the source at the observer, i.e.,

$$\mu_0 = \frac{d\Omega_I}{d\Omega_S} = (\frac{A_I}{D_L^2})(\frac{D_S^2}{A_S}) \tag{2.2.1}$$

A_I and A_S are the image area on the lens plane and source plane (figure 2.2.1) respectively.

If θ is the angular distance of the image from the optical axis and ϕ is the azimuthal angle, then the area of the image in the celestial sphere of the observer is given by,

$$A_I = D_L^2 \sin\theta d\theta d\phi$$

Since θ is small,

$$A_I = D_L^2 \theta d\theta d\phi .$$

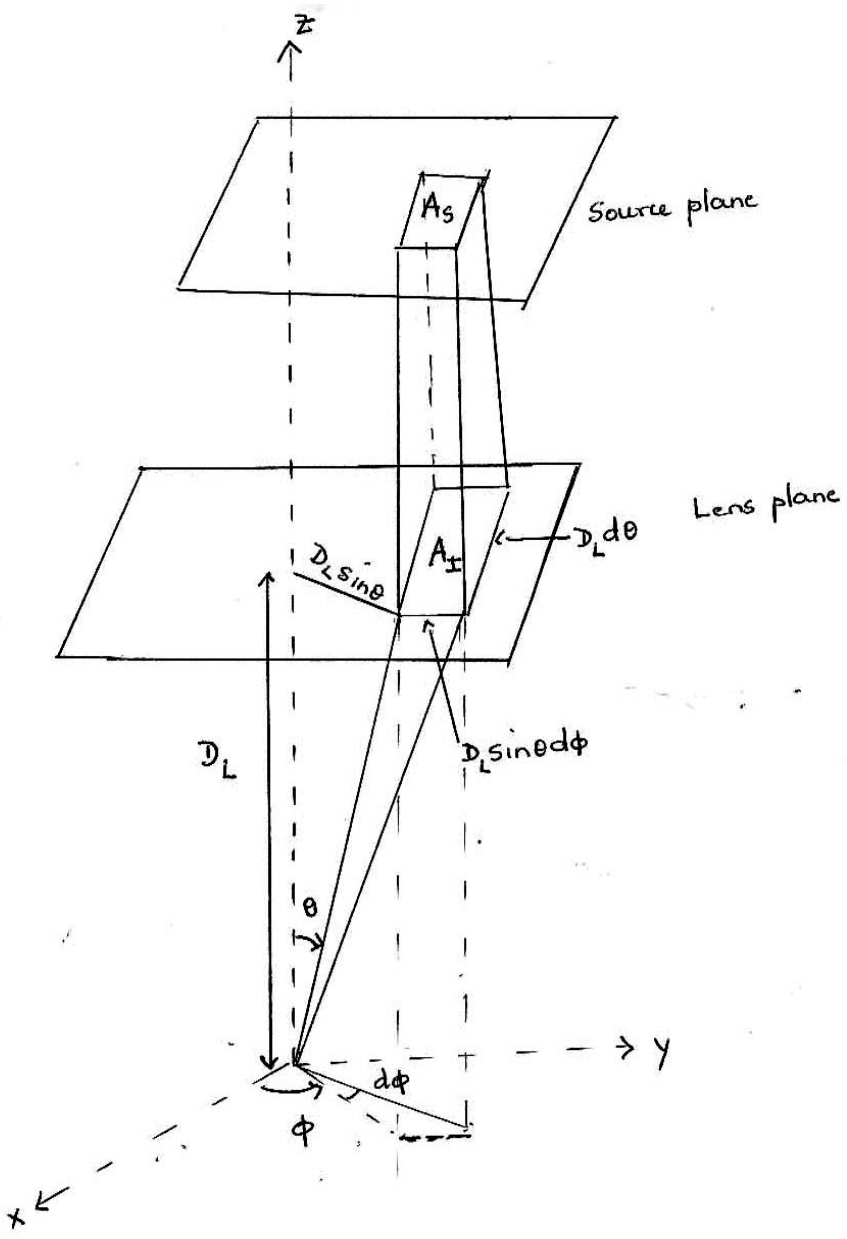

Figure 2.2.1 Illustration of source and image area

Similarly we can obtain the area of the source. Since the source is at an angular distance β then at distance D_S its area is,

$A_S = D_S^2 \beta d\beta d\phi$. Thus by the substitution of the source and lens areas into equation 2.2.1 we get,

$$\mu_0 = \frac{\theta d\theta}{\beta d\beta} \tag{2.2.2}$$

In the thin lens approximation, as we saw earlier, the lens equation can be written in terms of the angular distances of the source and the image, the deflection angle α, the Schwarzschild radius, $R_S = \frac{2GM}{c^2}$.

Since $\alpha = \frac{4GM}{c^2 \xi} = \frac{4GM}{c^2(\theta D_L)} = 2\frac{R_S}{\theta D_L}$, by substituting this into equation 2.1.2 for a spherically symmetric lens, we obtain the spherically symmetric thin lens equation in the form

$$\beta = \theta - \frac{2R_S D_{LS}}{\theta D_S D_L} \tag{2.2.3}$$

For this case, to determine the magnification as defined by equation 2.2.2, we differentiate equation 2.2.3 with respect to θ:

$$\frac{\partial \beta}{\partial \theta} = 1 + \frac{2R_S D_{LS}}{D_S D_L \theta^2}$$

$$\frac{\beta}{\theta}\frac{\partial \beta}{\partial \theta} = (1 - \frac{2R_S D_{LS}}{D_S D_L \theta^2})(1 + \frac{2R_S D_{LS}}{D_S D_L \theta^2}),$$

this leads to

$$\mu_0 = \frac{\theta d\theta}{\beta d\beta} = \frac{1}{(1 - \frac{4{R_S}^2 D_{LS}^2}{D_S^2 D_L^2 \theta^4})} \tag{2.2.4}$$

Since the impact parameter b in the lens plane, is given by

$D_L \theta = b$, by substituting this into equation 2.2.4, we get,

$$\mu_0 = (1 - \frac{4R_S^2 (D_S - D_L)^2 D_L^2}{b^4 D_S^2})^{-1}$$

$$= \frac{D_S^2}{D_S^2 - \frac{4R_S^2 D_L^2 (D_S - D_L)^2}{b^4}} \tag{2.2.5}$$

Equation 2.2.5 gives the magnification of the thin non-transparent lens in terms of the fixed lens parameters and the arbitrary impact parameter, b.

We now show how the magnification of a thin transparent lens is determined.

The magnification of the image can also be defined as the inverse of the determinant of the Jacobian matrix $\hat{A}$ of the lens mapping $\vec{\theta} \to \vec{\beta}$ (Schneider, Ehlers and Falco, 1992, Narayan and Bartelmann, 1996):

$$\mu = \left| \det \frac{\partial \vec{\beta}}{\partial \vec{\vartheta}} \right|^{-1} = \frac{D_S^2 A_I}{D_L^2 A_S} \tag{2.2.6}$$

In order to understand the physical significance of the elements of the Jacobian matrix, we need to define the "deflection potential". The deflection potential $\psi(\vec{\xi})$ is the projection of the Newtonian potential into the lens plane. From this deflection potential we can derive certain

entities that are relevant to gravitational lensing by taking a scaled potential that is related to the deflection potential, $\tilde{\psi} = \frac{D_{LS}\psi}{D_S D_L}$.

We define a scaled deflection angle that is related to the true deflection angle, $\vec{\tilde{\alpha}} = \frac{D_{DS}}{D_S}\vec{\alpha}$ and is given by the gradient of the scaled potential with respect to the angular position of the image, $\theta = (\theta_1, \theta_2)$,

$$\vec{\tilde{\alpha}} = \vec{\nabla}\tilde{\psi} \tag{2.2.7}$$

The elements of the Jacobian matrix $\hat{A}$ for a lens in general, are given by (Schneider et al. 1992) ,

$$A_{ij} = (\delta_{ij} - \frac{\partial^2 \tilde{\psi}}{\partial\theta_i \partial\theta_j}) \tag{2.2.8}$$

The second derivative of the scaled deflection potential in equation 2.2.8 reveals the deviation from the identity mapping due to the thin lens mapping. It also describes the convergence and the shear. The lensed image of a source can have the same shape as the source but be larger or smaller in size. This isotropic focusing effect is described by the convergence $\kappa(\theta)$. When the mapping is anisotropic and the shape of the image is different, e.g. elliptical rather than the spherical shape of the source, it is described by the shear $\gamma(\theta) \equiv (\gamma_1, \gamma_2)$.

The Laplacian of the deflection potential gives the convergence $\kappa(\theta)$ for a symmetric lens:

$$\nabla^2\psi(\theta) = 2\kappa(\theta) \tag{2.2.9}$$

If θ_1 and θ_2 are the components of the angular vector $\vec{\theta}$ in the lens plane, then the convergence and the shear can be determined from the deflection potential in the following manner,

$$\kappa(\theta) = \frac{1}{2}(\psi_{\theta_1\theta_1} + \psi_{\theta_2\theta_2}),$$

$$\gamma_1 = \frac{1}{2}(\psi_{\theta_1\theta_1} - \psi_{\theta_2\theta_2}) \;\; ; \gamma_2 = \psi_{\theta_2\theta_1}$$

The Jacobian matrix expressed in terms of the convergence and the shear is,

$$\hat{A} = \begin{pmatrix} 1-\kappa-\gamma_1 & -\gamma_2 \\ -\gamma_2 & 1-\kappa+\gamma_1 \end{pmatrix} \tag{2.2.10}$$

The determinant of $\hat{A}$ is used in the next section to obtain the transparent thin lens magnification.

2.3 THE PROJECTED SPHERICALLY SYMMETRIC THIN LENS (PSSTL)

In this section we derive the magnification for a thin transparent lens. In order to do this, we first find the projected mass on the lens plane of a spherically symmetric lens. Then determine the shear and convergence that would enable us to find the Jacobian matrix which would eventually lead to the determination of the magnification of the source.

For a spherically symmetric lens, (a) the source and the observer can be assumed to be coplanar with the optical axis, and the two dimensional vector $\xi = \left|\vec{\xi}\right|$; (b) the angular coordinates of the image $\theta_1 = \theta_2 = \theta$; (c) if the lens has a uniform mass density ρ and a radius R then the surface mass density is given by

$$\Sigma(\xi) = \int_{-\sqrt{R^2-\xi^2}}^{\sqrt{R^2-\xi^2}} \rho \, dz = 2\rho\sqrt{R^2 - \xi^2} \tag{2.3.1}$$

To make the surface mass density dimensionless a critical mass density is used which involves the distances of the GL system:

$$\Sigma_c = \frac{c^2 D_S}{4\pi G D_L D_{LS}} \tag{2.3.2}$$

For a spherically symmetric lens the scaled deflection angle $\tilde{\alpha}$ and potential $\tilde{\psi}$ (Schneider et al., chapter 8) both being a function of the angular position of the image $\theta = \frac{\xi}{D_L}$ are,

$$\tilde{\alpha}(\theta) = \frac{2}{\theta}\int_0^{\theta} \theta d\theta \kappa(\theta) \equiv \frac{m(\theta)}{\theta} \tag{2.3.3}$$

$$\tilde{\psi}(\theta) = 2\ln\theta \int_0^{\theta} \theta d\theta \kappa(\theta) \equiv m(\theta)\ln\theta \tag{2.3.4}$$

$$\text{where, } m(\theta) = 2\int_0^{\theta} \theta d\theta \frac{2\rho\sqrt{R^2 - (\theta D_L)^2}}{\Sigma_c} \tag{2.3.5}$$

$m(\theta)$ is the dimensionless mass within a circle of angular radius $\theta = (\theta_1, \theta_2)$.

Evaluating the integral in equation 2.3.5 we get

$$m(\theta) = \frac{4\rho R^3}{3\Sigma_c D_L^2}\left[1-(1-\frac{(\theta D_L)^2}{R^2})^{3/2}\right] \tag{2.3.6}$$

From the scaled deflection potential the shear can be obtained for a spherically symmetric lens and assuming θ is small;

$$\gamma_1 = \frac{1}{2}(\frac{\partial^2\tilde{\psi}}{\partial\theta_1{}^2} - \frac{\partial^2\tilde{\psi}}{\partial\theta_2{}^2}) = 0$$
$$\gamma_2 = \frac{\partial^2\tilde{\psi}}{\partial\theta_1\partial\theta_2} = \frac{\partial^2\tilde{\psi}}{\partial\theta^2} = \frac{m}{\theta^2} \tag{2.3.7}$$

The determinant of $\hat{A}$ in equation 2.2.10 is

$$\det\hat{A} = (1-\kappa)^2 - \gamma_1^2 - \gamma_2^2 \tag{2.3.8}$$

Substituting the shear components from equation 2.3.7 into 2.3.8 we get,

$$\det A = (1-\frac{m}{\theta^2})(1+\frac{m}{\theta^2}-2\kappa) \tag{2.3.9}$$

Incorporating the dimensionless mass from equation 2.3.6 into 2.3.9, we get,

$$\det\hat{A} = \left[1-\frac{4\rho}{3\Sigma_c\theta^2 D_L^2}\{R^3-(R^2-\theta^2 D_L^2)^{3/2}\}\right]$$
$$\text{x}\left[1+\frac{4\rho R^3}{3\Sigma_c\theta^2 D_L^2} - \frac{4\rho(R^2-\theta^2 D_L^2)^{3/2}}{3\Sigma_c\theta^2 D_L^2} - \frac{4\rho(R^2-\theta^2 D_L^2)^{1/2}}{\Sigma_c}\right]$$

Substituting the impact parameter $\xi = \theta D_L$, into the above equation we have,

$$\det \hat{A} = \left[1 - \frac{4\rho}{3\Sigma_c \xi^2} \{R^3 - (R^2 - \xi^2)^{3/2}\} \right]$$
$$\text{x} \left[1 + \frac{4\rho R^3}{3\Sigma_c \xi^2} - \frac{4\rho (R^2 - \xi^2)^{3/2}}{3\Sigma_c \xi^2} - \frac{4\rho (R^2 - \xi^2)^{1/2}}{\Sigma_c} \right] \qquad (2.3.10)$$

The inverse of the determinant of $\hat{A}$ in equation 2.3.10 is the magnification of the image of the source in the PSSTL model.

Summarizing, for an uniform density spherically symmetric lens,

$$\mu_0 = \frac{1}{\det A} \qquad (2.3.11)$$

For a transparent thin lens det $\hat{A}$ is given by equation 2.3.10 and for an opaque thin lens,

$$\mu_0 = \frac{D_S^2}{D_S^2 - \dfrac{4R_S^2 D_L^2 (D_S - D_L)^2}{b^4}} \qquad (2.3.12)$$

here $b = \xi$ is the impact parameter and R_S is the Schwarzschild radius.

3.0 THE THICK LENS MODEL

In our thick lens model we consider the past light cone of the observer where all null geodesics originating at the observer initially travel backwards in time through flat space. As they approach the lens, the space-time curvature changes in a finite region from zero to a non-zero value governed by the space-time metric of the lensing mass. The solution to the geodesic deviation equation gives the deviation between two neighboring null rays in regions of flat space and non-zero curvature. We first derive in section 3.1 the geodesic deviation equation in the form that is applicable to our model.

The geodesic deviation equation has a different structure for a transparent lens than from a non-transparent one. In one there is both Ricci and Weyl tensor while in the other just Weyl tensor. In section 3.2 we solve the deviation equation for the non-transparent lens and in section 3.3 we do the same for the transparent lens. Finally in section 3.4 we explain the derivation of the thick lens magnification and compare it with the thin lens magnification in the vacuum region.

3.1 THE NULL GEODESIC DEVIATION EQUATION

Let an observer be at rest in the local coordinates x^a in a four dimensional space-time $(M, g_{ab}(x^a)$, with signature of (1,-1,-1,-1). The world line of the observer is given by $x_0^a(\tau)$ where τ is the proper time of the observer. The observer views the source on his or her celestial sphere (associated with the observers past light cone) with (stereographic) angular coordinates $\zeta, \overline{\zeta}$. The parameter length of the geodesics that generate the past cone are the affine length s. These null geodesics can be described by the curve, $x^a = Y^a(x_0^a(\tau), s, \zeta, \overline{\zeta})$, which satisfies the geodesic equation,

$$l^a \nabla_a l^b = 0 \qquad 3.1.1$$

with the null condition $g_{ab} l^a l^b = 0$. Here l^a is the tangent to the geodesics and is given by the derivative of Y^a with respect to the affine length s. The derivative of Y^a with respect to the angular coordinates $\zeta, \overline{\zeta}$, give the connecting vectors of the neighboring null geodesics:

$$l^a = \frac{\partial Y^a}{\partial s} \qquad 3.1.2$$

$$M_1{}^a = (1 + \zeta\overline{\zeta})\frac{\partial Y^a}{\partial \zeta} \qquad 3.1.3a$$

$$M_2{}^a = (1 + \zeta\overline{\zeta})\frac{\partial Y^a}{\partial \overline{\zeta}} \qquad 3.1.3b$$

$M_1{}^a$ and $M_2{}^a$ are, in general, linearly independent Jacobi fields that are orthogonal to l^a such that

$$g_{ab} M_1^a l^b = 0$$
$$g_{ab} M_2^a l^b = 0$$

Let us define a pair of independent, complex, orthonormal space-like vectors ($m^a, \overline{m}^a$), that are parallel propagated along the null geodesic tangent to l^a.

The Jacobi fields (M_1^a, M_2^a) can now be expressed in terms of the space-like vectors ($m^a, \overline{m}^a$) in the transverse direction and a longitudinal component along l^a.

$$\therefore M_1{}^a \equiv \xi m^a + \eta \overline{m}^a + \nu l^a \qquad 3.1.4a$$

$$\therefore M_2{}^a \equiv \overline{\eta} m^a + \overline{\xi}\,\overline{m}^a + \overline{\nu} l^a \qquad 3.1.4b$$

Our interest is in the deviation vector, therefore the component of $M_1{}^a, M_2^a$ along the tangent, l^a can be ignored and only the orthogonal components to l^a will be considered.

The connecting vectors M^a, satisfies the geodesic deviation equation

$$l^c \nabla_c l^b \nabla_b M^a = R_{bcd}{}^a l^b M^c l^d \qquad 3.1.5$$

where R_{abcd} is the curvature tensor, and can be rewritten in terms of the components of equations 3.1.4a and 3.1.4b as a complex 2x2 matrix

$$\hat{X} = \begin{pmatrix} \xi & \overline{\eta} \\ \eta & \overline{\xi} \end{pmatrix} \qquad 3.1.6$$

The curvature tensor R_{abcd} can be written in the form of a curvature matrix $\hat{Q}$, represented by

$$\hat{Q} = \begin{pmatrix} \Phi_{00} & \overline{\Psi}_0 \\ \Psi_0 & \Phi_{00} \end{pmatrix} \qquad 3.1.7$$

The elements of the curvature matrix are

$$\Phi_{00} = \frac{1}{2} R_{ab} l^a l^b \qquad 3.1.8$$

where R_{ab} is the Ricci tensor and

$$\Psi_0 = C_{abcd} l^a m^b l^c m^d \qquad 3.1.9$$

where C_{abcd} is the Weyl tensor.

In terms of $\hat{X}$, $\hat{Q}$ and $D = \frac{d}{ds}$, the geodesic deviation equation (3.1.5) becomes the 2x2, second order matrix differential equation,

$$D^2 \hat{X} = -\hat{Q}\hat{X} \qquad 3.1.10$$

Our primary objective is to solve equation (3.1.10) for the deviation along a single null geodesic traveling from the observer (s = 0) to the source (s = s*). In between the observer and the source the null geodesic may encounter a distribution of matter which in turn creates, via the Einstein equations, curvature in the form of Ricci and Weyl tenors that is the gravitational lens

lying along the line of sight of the observer. In the next section we seek and find solutions to equation (3.1.10) for a non-transparent lens only in the Weyl tensor region.

3.2 THE OPAQUE LENS

When the lens is opaque, the trajectory of the null geodesic travels first and last through flat space regions far from the lens; these regions will be labeled as I on the observer side and III on the source side. Closer to the lens it passes through the constant curvature vacuum region, identified as region II. Figure 3.2.1 illustrates the different regions.

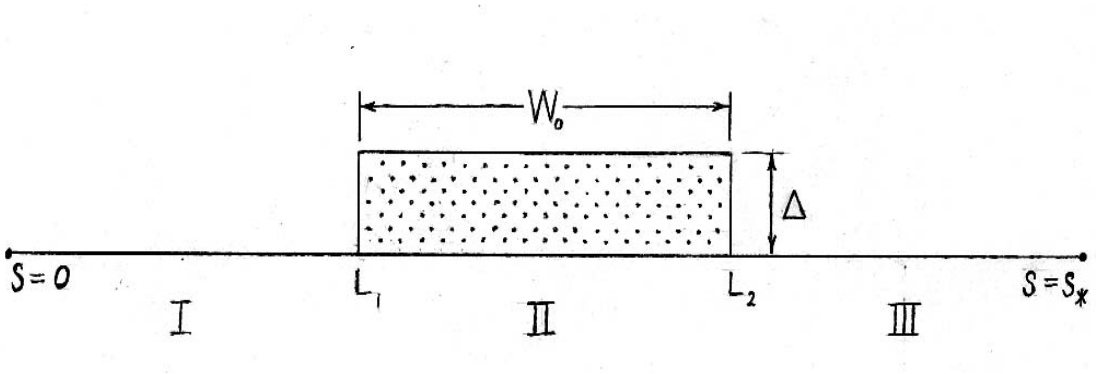

Figure 3.2.1 Model of an opaque lens

The geodesic deviation equation will differ in region II from I and III because the curvature matrix varies when the light rays travel through regions of non-vanishing space-time curvature. In Region I and III, the assumption of flat space means both the Weyl curvature and the Ricci tensor are zero,

$$\Phi_{00} = 0, \Psi_0 = 0 \qquad 3.2.1$$

so that the geodesic deviation equation for region I and III is

$$D^2 \hat{X} = 0 \qquad 3.2.2$$

In the vacuum region II near the lens, the space-time curvature is non-vanishing therefore,

$$\Phi_{00} = 0, \Psi_0 \neq 0 \qquad 3.2.3$$

and the geodesic deviation equation in region II becomes

$$D^2 \hat{X} = -\begin{pmatrix} 0 & \overline{\Psi}_0 \\ \Psi_0 & 0 \end{pmatrix} \hat{X} \qquad 3.2.4$$

We seek solutions to the geodesic deviation equations 3.2.2 in region I (the observer side), with the following initial conditions. Null geodesics of the observer's past null cone have their apex at the observer so the deviation matrix $\hat{X}$ must vanish at the observer.

$$\therefore \hat{X} = 0 \text{ at s=0} \qquad 3.2.5$$

The orthonormality condition for the connecting vectors at the observer force the initial condition on the first derivatives,

$$D\hat{X}_I = \begin{pmatrix} 1 & 0 \\ 0 & 1 \end{pmatrix} \text{ at s=0} \qquad 3.2.6$$

In region II we solve equation 3.2.4 and in III equation 3.2.2 with the boundary condition that $\hat{X}$ and its first derivative must be continuous across the boundaries of all the three regions:

$$\hat{X}_i(L_i) = \hat{X}_{i+1}(L_i), i = 1...2 \qquad 3.2.7$$

$$D\hat{X}_i(L_i) = D\hat{X}_{i+1}(L_i), i = 1...2 \qquad 3.2.8$$

We write the component of the Weyl tensor, Ψ_0 as

$$\Psi_0 = \Delta e^{if} \tag{3.2.9}$$

and refer to Δ as the height or strength of the Weyl. f is a phase factor depending on the initial choice of m^a. In regions of constant curvature II we will take a constant value of Δ.

As mentioned earlier we choose lenses with spherical symmetry so that the exterior regions of such lenses can be described by the Schwarzschild metric:

$$ds^2 = (1-2m/r)dt^2 - \frac{dr^2}{(1-2m/r)} - r^2(d\theta^2 + \sin^2\theta d\phi) \tag{3.2.10}$$

where $m = \frac{GM}{c^2}$ and M is the mass of the lens.

The components of the Weyl tensor in the radial null tetrad coordinate were determined by Janis and Newman (1965), Todd and Newman (1980):

$$\Psi_0 = \Psi_1 = \Psi_3 = \Psi_4 = 0, \Psi_2 = \frac{GM}{c^2 r^3} \tag{3.2.11}$$

In order to apply this to lensing we must transform the components of the Weyl tensor from radial to a null tetrad chosen along the null geodesic in the observer's past light cone. The construction of this transformation is given in appendix A. From it we find the Weyl tensor component Ψ_0, given in the appropriate tetrad system that is associated with our null geodesic. It takes the form

$$\Psi_0 = f(z,b)\frac{GM}{c^2 r^3} \tag{3.2.12}$$

The variable b is the impact parameter while z represents the orthogonal distance along the geodesic from the impact parameter. (See figure 3.2.2.) The function f (z, b) has the form

$$f(z,b) = \frac{3\{1 + 2(z/b)^2 + 2(z/b)(1 + (z/b)^2)^{1/2}\}}{\{1 + 3(z/b)^2 + 2(z/b)^4 + 2(z/b)(1 + (z/b)^2)^{3/2}\}} \quad \text{.....3.2.13}$$

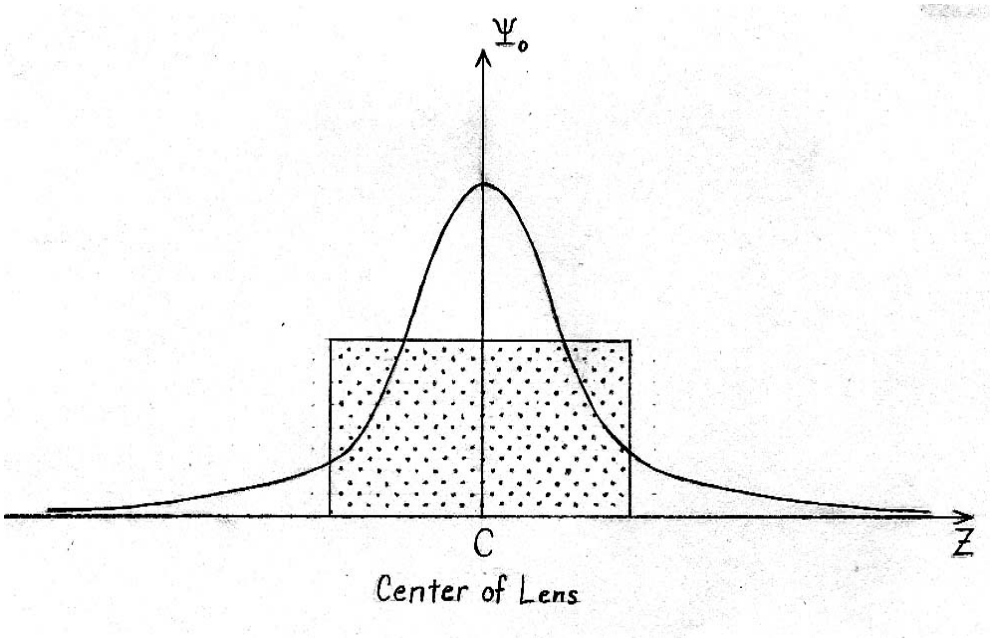

Figure 3.2.2 Determination of the height of the Weyl tensor

In order to assign a constant width w_0 to the non-vanishing Weyl region Ψ_0, we chose (arbitrarily) a spherical region of radius twice that of the matter region of the lens R_0. From this we determined the width;

$$w_0 = 2\sqrt{4R^2 - b^2} \qquad 3.2.14$$

To obtain the height Δ, we integrated Ψ_0 (equation 3.2.12) over the entire path of the null geodesic for each particular value of the impact parameter b, see figure 3.2.2. The average area under this curve gave us the estimate of the height Δ:

$$\Delta = \frac{\int_{-\infty}^{\infty} \Psi_0 dz}{w_0} \qquad 3.2.15$$

Using 3.2.14 and solving the geodesic equations in the three regions with the initial conditions and the continuity conditions between the regions we finally obtain the full solution in region III at the source. The solution $\hat{X}_{III}$ is given by

$$\hat{X}_{III} = \begin{pmatrix} g_1 & g_2 \\ \bar{g}_2 & g_1 \end{pmatrix} s_* + \begin{pmatrix} f_1 & f_2 \\ \bar{f}_2 & f_3 \end{pmatrix} \qquad 3.2.16$$

$$g_1 = 0.5L_1\sqrt{\Delta}(\sinh w - \sin w) + 0.5(\cosh w + \cos w)$$
$$g_2 = -0.5L_1\sqrt{\Delta}(\sinh w + \sin w) + 0.5(\cos w - \cosh w)$$
$$f_1 = 0.5\{(L_1 - L_2)(\cosh w + \cos w) + (\frac{1}{\sqrt{\Delta}} - L_1L_2\sqrt{\Delta})\sinh w + (\frac{1}{\sqrt{\Delta}} + L_1L_2\sqrt{\Delta})\sin w\}$$
$$f_2 = 0.5\{(L_1L_2\sqrt{\Delta} - \frac{1}{\sqrt{\Delta}})\sinh w + (L_2 - L_1)(\cosh w - \cos w) + (L_1L_2\sqrt{\Delta} + \frac{1}{\sqrt{\Delta}})\sin w\}$$

3.2.17

$$L_1 = D_S - \frac{w_0}{2},\ \mathrm{L}_2 = D_S + \frac{w_0}{2},\ w = w_0\sqrt{\Delta}$$

From this solution we will show, in section 3.2.4, how the opaque thick lens magnification can be determined.

3.3 THE TRANSPARENT LENS

When null geodesics pass through a transparent lens we have five different regions to consider as shown in figure 3.3.1. The curvature matrix $\hat{Q}$ varies as the null geodesic moves

through regions of different space-time curvature, consequently the geodesic deviation equation changes too.

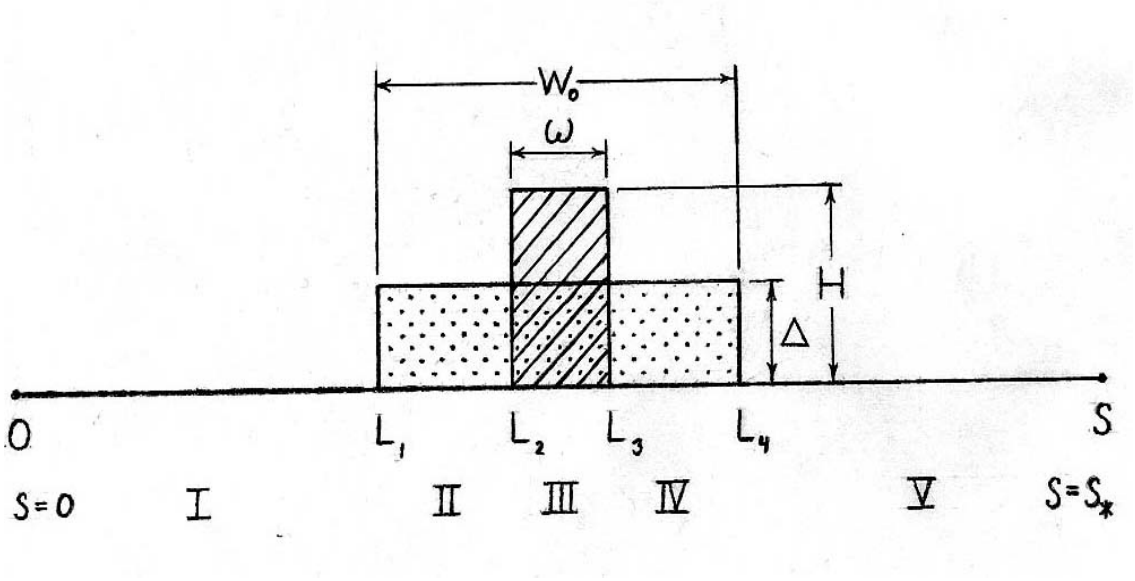

Figure 3.3.1 Model of a transparent lens

In the far zones I (observer side) and V (source side), $\hat{Q} = 0$ because of flat space and the geodesic deviation equation is identical to equation 3.2.2.

Region II and IV are the near zone outside the lens mass where we assume constant Weyl curvature but no Ricci tensor (or mass), therefore in these two regions $\Phi_{00} = 0, \Psi_0 \neq 0$.

In these two zones the deviation equation is the same as equation 3.2.4.

In region III the null geodesic encounters the mass of the lens and a constant Weyl curvature, hence here $\Phi_{00} \neq 0, \Psi_0 \neq 0$. For region III, the geodesic deviation equation is

$$D^2 \hat{X} = -\begin{pmatrix} \Phi_{00} & \overline{\Psi}_0 \\ \Psi_0 & \Phi_{00} \end{pmatrix} \hat{X} \qquad 3.3.1$$

To solve the geodesic deviation equation in region I we applied the same initial conditions as equations 3.2.5 and 3.2.6. The boundary conditions are similar to equations 3.2.7 and 3.2.8, except that in this case we have to match the continuity of the solution and its first derivative across four boundaries. Therefore,

$$\hat{X}_i(L_i) = \hat{X}_{i+1}(L_i), i = 1...4 \qquad 3.3.2$$

$$D\hat{X}_i(L_i) = D\hat{X}_{i+1}(L_i), i = 1...4 \qquad 3.3.3$$

The component of the Weyl tensor, Ψ_0 is again written as

$\Psi_0 = \Delta e^{if}$. Δ, the height of the Weyl curvature is taken constant across the regions II, III and IV. The determination of Δ is different from that of a non-transparent lens. Ψ_0 is a piecewise continuous function. In the regions II and IV, Ψ_0 is determined in the same manner as the opaque lens:

$$\Psi_0 = \frac{GM_{total}}{c^2 r^3} f(z,b), \; R_0 \le r \le 2R_0 \qquad 3.3.4$$

where r is the radial coordinate given by, $r = \sqrt{z^2 + b^2}$, $2\mathrm{R}_0 \ge \mathrm{b} \ge \mathrm{R}_0$.

In region III, the null rays encounter the mass of the lens. The Weyl component Ψ_0 is a function of the mass M within a radius r given by

$r = \sqrt{z^2 + b^2}$, $\mathrm{b} \le \mathrm{R}_0$

$$\Psi_0 = \frac{GM}{c^2 r^3} f(z,b), \; r \le |R_0| \qquad 3.3.5$$

The function f(z, b) has the same form as equation 3.2.12

In order to assign a constant width and a constant height to this Ψ_0, Ψ_0 was integrated over the entire path of the null geodesic for a particular value of the impact parameter b and the area under this curve gave us the height Δ (see figure 3.3.2)

.

$$(\Delta)(w_0) = \int_{-\infty}^{+\infty} \Psi_0 dz \qquad 3.3.6$$

The width w_0 depends on the assumed extent of the Weyl curvature (figure 3.3.2)

We assume the Weyl curvature is nonzero over a spherical region of radius $2R_0$. Therefore the width is given by

$$w_0 = 2(4R_0{}^2 - b^2)^{1/2} \text{ when } b < R_0 \qquad 3.3.7$$

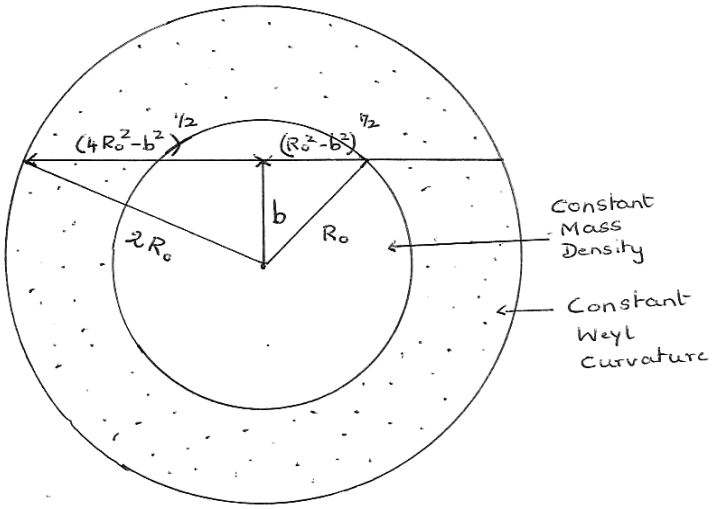

Figure 3.3.2 Determination of width of the Weyl and Ricci tensors

To find the height Δ when b < R_0 equation 3.3.6 is integrated piecewise across the vacuum region II, the matter dominated region III and then the vacuum region IV:

$$\Delta w_0 = \int_{-\infty}^{-(R_0^2-b^2)^{1/2}} (\Psi_0)_{opaque} dz + \int_{-(R_0^2-b^2)^{1/2}}^{(R_0-b^2)^{1/2}} (\Psi_0)_{transparen} dz + \int_{(R_0^2-b^2)^{1/2}}^{\infty} (\Psi_0)_{opaque} dz \qquad 3.3.8$$

$(\Psi_0)_{opaque}$ is given by equation 3.3.4 and $(\Psi_0)_{transparent}$ by equation 3.3.5.

To obtain the Ricci tensor Φ_{00} in the geodesic deviation equation 3.3.1 we assume that the transparent lenses are made of non-interacting fluid matter of constant density. The matter field is characterized by the velocity and the density. The velocity is given by $u^a = \frac{dx^a}{d\tau}$, where τ is the proper time of the world line of a particle and if ρ_0 is the proper density of the flow, then the energy-momentum tensor T_{ab} for the matter field is given by

$$T^{ab} = \rho_0 u^a u^b \quad \text{where } u^a = \gamma(1, \vec{v})$$

$$\gamma = \frac{1}{\sqrt{(1-\frac{v^2}{c^2})}}. \text{, } u = (1, 0) \qquad 3.3.9$$

Einstein's field equation is

$$R_{ab} - \frac{g_{ab}R}{2} = \frac{8\pi G T_{ab}}{c^2} \qquad 3.3.10$$

R_{ab} is the Ricci tensor and R is the Scalar Curvature.

Contracting equation 3.3.10 with the tangent to the geodesic, l^a we get,

$$R_{ab}l^a l^b = \frac{8\pi G T_{ab} l^a l^b}{c^2} \text{ with } l^a = (1,0,0,1) \qquad 3.3.11$$

$$\Phi_{00} \equiv \frac{1}{2} R_{ab} l^a l^b \qquad 3.3.12$$

Substituting equations 3.3.12 and 3.3.9 into equation 3.3.12, we get,

$$\Phi_{00} = \frac{4\pi G \rho_0}{c^2} = \frac{3GM_{total}}{c^2 R_0{}^3} \equiv H \qquad 3.3.13$$

Since we assume that the lens has a uniform density the height H of the Ricci tensor will be independent of the impact parameter but the width will be dependent on b and is given by $\omega = 2\sqrt{R_0^2 - b^2}.$

The solution to the geodesic deviation equation in region V is given by

$$\hat{X}_V = \begin{pmatrix} g_1 & g_2 \\ \bar{g}_2 & g_1 \end{pmatrix} s_* + \begin{pmatrix} f_1 & f_2 \\ \bar{f}_2 & f_3 \end{pmatrix},$$

where $g_{1,} g_2$, $f_{1,} f_2$ are written in terms of the quantities:

$$u \equiv \sqrt{\Delta}(L_4 - L_3) = \sqrt{\Delta}(\sqrt{(4R_0^2 - b^2)} - \sqrt{R_0^2 - b^2})$$
$$v \equiv \sqrt{\Delta - H}\,(L_3 - L_2) = \sqrt{\Delta - H}\,(2\sqrt{R_0^2 - b^2}$$
$$w \equiv \sqrt{\Delta}(L_2 - L_1) = \sqrt{\Delta}(\sqrt{(4R_0^2 - b^2)} - \sqrt{R_0^2 - b^2})$$
$$v_0 \equiv \sqrt{\Delta - H}\,(L_3 - L_2) = \sqrt{\Delta - H}\,(2\sqrt{R_0^2 - b^2})$$

$$L_4 = D_L + \sqrt{(4R_0^2 - b^2)}$$
$$L_3 = D_L + \sqrt{(R_0^2 - b^2)}$$
$$L_2 = D_L - \sqrt{(R_0^2 - b^2)}$$
$$L_1 = D_L - \sqrt{(4R_0^2 - b^2)}$$

as

$$\begin{aligned} g_1 = {} & 0.5\left[(\Delta - H)^{1/2}\cosh u \sinh v + (\Delta)^{1/2}\sinh u \cosh v\right]\left[L_1 \cosh w + (\Delta)^{-1/2}\sinh w\right] \\ & + 0.5\left[(\Delta - H)^{1/2}\cosh u \cosh v + (\Delta)^{1/2}\sinh u \sinh v\right] \\ & \left[(\Delta - H)^{-1/2}\cosh w + L_1(\Delta/(\Delta - H))^{1/2}\sinh w\right] \\ & + 0.5\left[-(\Delta)^{1/2}\sin u \cos v_0 - (\Delta + H)^{1/2}\cos u \sin v_0\right]\left[L_1 \cos w + (\Delta)^{1/2}\sin w\right] \\ & + 0.5\left[-(\Delta)^{1/2}\sin u \sin v_0 + (\Delta + H)^{1/2}\cos u \cos v_0\right] \\ & \left[(\Delta + H)^{1/2}\cos w - L_1(\Delta/(\Delta + H))^{1/2}\sin w\right] \end{aligned}$$

$$\begin{aligned} g_2 = {} & -0.5\left[(\Delta - H)^{1/2}\cosh u \sinh v + (\Delta)^{1/2}\sinh u \cosh v\right]\left[L_1 \cosh w + (\Delta)^{-1/2}\sinh w\right] \\ & - 0.5\left[(\Delta - H)^{1/2}\cosh u \cosh v + (\Delta)^{1/2}\sinh u \sinh v\right] \\ & \left[(\Delta - H)^{-1/2}\cosh w + L_1(\Delta/(\Delta - H))^{1/2}\sinh w\right] \\ & + 0.5\left[-(\Delta)^{1/2}\sin u \cos v_0 - (\Delta + H)^{1/2}\cos u \sin v_0\right]\left[L_1 \cos w + (\Delta)^{1/2}\sin w\right] \\ & + 0.5\left[-(\Delta)^{1/2}\sin u \sin v_0 + (\Delta + H)^{1/2}\cos u \cos v_0\right] \\ & \left[(\Delta + H)^{1/2}\cos w - L_1(\Delta/(\Delta + H))^{1/2}\sin w\right] \end{aligned}$$

and

$$f_1 = 0.5\left[(\Delta - H)^{1/2}\sinh v\{\frac{\sinh u}{\sqrt{\Delta}} - L_4\cosh u\} + \cosh v\{\cosh u - L_4\sqrt{a}\sinh u\}\right]$$
$$\left[L_1\cosh w + (\Delta)^{1/2}\sinh w\right]$$
$$+ 0.5\left[(\Delta - H)^{1/2}\cosh v\{\frac{\sinh u}{\sqrt{\Delta}} - L_4\cosh u\} + \sinh v\{\cosh u - L_4(\Delta)^{1/2}\sinh u\}\right]$$
$$\left[(\Delta - H)^{-1/2}\cosh w + (\Delta/(\Delta - H))^{1/2}L_1\sinh w\right]$$
$$+ 0.5\left[\cos v_0\{\cos u + L_4(\Delta)^{1/2}\sin u\} - (\Delta + H)^{1/2}\sin v_0\{(\Delta)^{-1/2}\sin u - L_4\cos u\}\right]$$
$$\left[L_1\cos w + (\Delta)^{-1/2}\sin w\right]$$
$$+ 0.5\left[\sin v_0\{\cos u + L_4(\Delta)^{1/2}\sin u\} + (\Delta + H)^{1/2}\cos v_0\{(\Delta)^{-1/2}\sin u - L_4\cos u\}\right]$$
$$\left[(\Delta + \mathrm{H})^{-1/2}\cos w - L_1(\Delta/(\Delta + M))^{1/2}\sin w\right]$$

$$f_2 = -0.5\left[(\Delta - H)^{1/2}\sinh v\{\frac{\sinh u}{\sqrt{\Delta}} - L_4\cosh u\} + \cosh v\{\cosh u - L_4\sqrt{a}\sinh u\}\right]$$
$$\left[L_1\cosh w + (\Delta)^{-1/2}\sinh w\right]$$
$$- 0.5\left[(\Delta - H)^{1/2}\cosh v\{\frac{\sinh u}{\sqrt{\Delta}} - L_4\cosh u\} + \sinh v\{\cosh u - L_4(\Delta)^{1/2}\sinh u\}\right]$$
$$\left[(\Delta - H)^{-1/2}\cosh w + (\Delta/(\Delta - H))^{1/2}L_1\sinh w\right]$$
$$+ 0.5\left[\cos v_0\{\cos u + L_4(\Delta)^{1/2}\sin u\} - (\Delta + H)^{1/2}\sin v_0\{(\Delta)^{-1/2}\sin u - L_4\cos u\}\right]$$
$$\left[L_1\cos w + (\Delta)^{-1/2}\sin w\right]$$
$$+ 0.5\left[\sin v_0\{\cos u + L_4(\Delta)^{1/2}\sin u\} + (\Delta + H)^{1/2}\cos v_0\{(\Delta)^{-1/2}\sin u - L_4\cos u\}\right]$$
$$\left[(\Delta + \mathrm{H})^{-1/2}\cos w - L_1(\Delta/(\Delta + M))^{1/2}\sin w\right]$$

In the next section we will see that the magnification can be found from this solution in the case of the transparent lens.

3.4 THE MAGNIFICATION OF THE SOURCE IN THE THICK LENS

In our model where we consider the observer's past light cone and the geodesic deviation equation with the initial conditions at the observer, $\hat{X} = 0$ and $D\hat{X} = \begin{pmatrix} 1 & 0 \\ 0 & 1 \end{pmatrix}$, Frittelli et al. (2002) showed that this implied that the solid angle of the image at the observer was normalized to be one. By choosing, $D_S = s_*$, the magnification of the source in the thick lens model is then, in general, given by,

$$\mu_T = \frac{\Omega_I}{\Omega_S} = \frac{1}{\frac{A_S}{s^2{}_*}} = \frac{s_*{}^2}{\det \hat{X}_s}$$

where X_s is the solution to the geodesic deviation equation at the source.

The magnification of the image for a transparent lens is given by the inverse of the determinant of $\hat{X}_V$,

$$\mu_T = \frac{s_*^2}{\det \hat{X}_V} \qquad 3.4.1$$

while for an opaque lens is given by

$$\mu_T = \frac{s_*^2}{\det \hat{X}_{III}} \qquad 3.4.2$$

For a transparent lens, when the null geodesics have impact parameter greater than the radius of the lens, we use equation 3.4.2 to determine the source magnification. When the

impact parameter for a null ray is less than the radius of the lens, we use equation 3.4.1 to find the magnification.

We can make a comparison of the thick versus thin lens magnification for null geodesic having an impact parameter $b > R_0$ in the following manner. In appendix B we show that the thick lens magnification can be expanded about the thin lens magnification μ_0 for small widths w_0 as

$$\mu_T = \mu_0 + w_0 Lt_{w_0 \to 0}\left(\frac{d\mu_0}{dw_0}\right) = \frac{s_*^2}{s_*^2(1-L_1^2J^2) + 2J^2L_1^3 s_* - J^2L_1^4} \qquad 3.4.3$$

where J is

$$J \equiv \Delta w_0 = \frac{4GM}{c^2b^2} = \frac{2R_S}{b^2} \qquad 3.4.4$$

Hence in the thick opaque lens the source magnification can be compared with the thin opaque lens as $w_0 \to 0$ in equation 3.4.3. To compare equation (3.4.3) with the thin lens magnification given in (2.3.12), we take $L_1 = L_2 = D_L$. Substituting 3.4.4 for J and $s_* = D_S$, equation 3.4.3 can be rewritten as,

$$\mu_T = \frac{D_S^2}{D_S^2\left(1 - \frac{4D_L^2R_S^2}{b^4}\right) + \frac{8R_S^2D_L^3D_S}{b^4} - 4\frac{R_S^2D_L^4}{b^4}}$$

$$= \frac{D_S^2}{D_S^2 - \frac{4R_S^2D_L^2(D_S - D_L)^2}{b^4}}$$

which is exactly the thin lens magnification. We thus see that our thick lens magnification goes smoothly to the thin lens as the thickness goes to zero.

By putting in detailed numbers later, into equation 3.4.3, we can see that there is little or no disagreement between the thick and thin lens magnification for impact parameters far from the Einstein radius, i.e., far from regions of high magnification. The correction term becomes large for impact parameters near the Einstein radius.

4.0 IDEALIZED TRANSPARENT LENSES AND THEIR PARAMETERS

In this chapter we study and compare the thick versus the thin lens models in several cases of idealized spherically symmetric transparent lenses with lensing parameters that lie in reasonable astrophysical ranges. Though for most situations they are unphysical (with a few real exceptions), we work out and compare the thin and thick lensing magnifications and the locations of the critical regions for several transparent astrophysical objects. This is done largely for the sake of simply understanding the mathematics of lensing in a transparent object.

In the thin lens map described in chapter 2 the magnification μ_0 is known for light rays that lie outside the lens. But the lenses that are considered here are transparent and the null geodesics can pass through the lens. To compare the image magnification of the thick lens μ_T with the thin lens for rays that pass through the transparent lens, we use the PSSTL model described in chapter 2. A description of certain lensing parameters for interior regions is given in 4.1. The mass of the theoretical lenses studied here is taken to be 10^{12} M_{sun} , a value similar to our Milky Way Galaxy. The distances are chosen to be comparable to those of observed galactic lensing systems. The thick lens parameters are defined in section 4.2. In 4.3 we give the definition of caustics and critical points. In 4.4 we examine four examples of gravitational lensing of a source due to a lens of constant mass but with 4 values of the radius. This allows us to test, what role the density of the transparent lens plays in the magnification in both thick and

thin lens models. The relationship between the density and the magnification is analyzed in section 4.5.

4.1 GRAVITATIONAL LENSING PARAMETERS

For the study of lensing by a transparent astrophysical object we review below four parameters that are relevant when the null geodesics pass through the interior of the lens. The Einstein radius is the exception, it is important for geodesics both passing outside and inside the lens.

These parameters are,

(i) the surface mass density Σ , which is the projection of the volume mass density of the lens onto the lens plane;

(ii) the Einstein radius R_E , which is the particular value of the impact parameter (in the vacuum region) that would theoretically give infinite magnification of the image when the source is located on the optical axis;

(iii) the critical surface mass density Σ_{cr} , which is the ratio of the mass of the lens to the area enclosed by the Einstein radius;

(iv) the dimensionless surface mass density κ , also known as the convergence.

For a spherically symmetric lens of uniform mass density ρ and radius R, the surface mass density is given by

$$\Sigma(b)=\int_{-\sqrt{R^2-b^2}}^{\sqrt{R^2-b^2}}\rho\,dz=2\rho\sqrt{R^2-b^2} \qquad 4.1.1$$

Here b is the impact parameter and z is chosen as the Cartesian coordinate parallel to the line of sight and transverse to b.

The Einstein radius is a function of the mass M of the lens, the distances to the source D_S, and lens D_L, from the observer, and the distance between the lens and the source D_{LS};

$$R_E = \sqrt{\frac{4GMD_L D_{LS}}{c^2 D_S}} \tag{4.1.2}$$

The critical surface mass density also depends on the variables described above, except that it is independent of the mass;

$$\Sigma_{cr} = \frac{c^2 D_S}{4\pi G D_L D_{LS}} \tag{4.1.3}$$

For a fixed lens and source location, the dimensionless surface mass density κ is a function of the impact parameter b;

$$\kappa(b) = \frac{\Sigma(b)}{\Sigma_{cr}} \tag{4.1.4}$$

The parameter κ establishes the criteria for multiple imaging. When

$$\kappa > 1 \tag{4.1.5}$$

the lens will give a large magnification of the image for four (two on either side of the optical axis) values of the impact parameters. For

$$\kappa < 1 \tag{4.1.6}$$

the lens will not cause any large magnification of the image.

$$\kappa \approx 1 \tag{4.1.7}$$

is interesting since this value of kappa separates the two cases where the Einstein radius of the lens lies either outside or inside the lens. We will discuss the effect of such lenses on the magnification in section 4.4.

4.2 THE THICK LENS PARAMETERS

The numerical values of the astrophysical parameters for the four cases that are discussed in this section are given below. In appendix C we show the derivation of the cosmological distances that are chosen here.

The parameters that are kept constant are:

M = the total mass of the lens = 10^{12} x M_{Sun} =2 x 10^{42} kg;

The Einstein radius, R_E = 0.3616 x 10^{18} km;

The Schwarzschild radius, $R_S = \frac{2GM}{c^2}$ = 2.96 x 10^{12} km;

The distance between source and observer, D_S = 2868 Mpc = 8.86 x 10^{22} km;

The distance between lens and observer, D_L = 1348 Mpc = 4.16 x 10^{22} km;

The distance of the source from the lens, D_{LS} = 1558 Mpc = 4.8 x 10^{22} km;

The minimum value of the impact parameter, $b_{\min} = 100 R_S$.

The one parameter that is varied is the radius of the lens R_0 . As a consequence the mass density of the lens ρ as well as the Ricci tensor $\Phi_{00} = \frac{4\pi\rho G}{c^2}$ also varies. We take four different values for R_0 .

4.3 CRITICAL POINTS AND CAUSTICS

When the determinant of A, the Jacobian of the lens map, is close to zero, the image magnification is extremely large. The locations of the source in the source plane, at which the magnification of the image is large, are the "caustics". The corresponding positions for the image in the image plane are referred to as the "critical points". The magnification changes sign when the impact parameter crosses a critical point. When the determinant A has a positive value, the image is said to have a positive parity and a negative parity when the determinant of A has a negative value. The Einstein radius of a lens is situated at a critical point if it is larger than the radius of the lens. There is some ambiguity about its meaning when the Einstein radius lies within the lens.

For the four examples of a lens that we consider in this section with constant mass but different radii we compute the magnification in the thin lens model (rays exterior to lens) and PSSTL model (rays interior to lens) and make a comparison with the thick lens model for

(i) the magnification at each impact parameter $\xi = b_i$, and

(ii) the location of the critical points.

4.4 CONSTANT MASS LENSES

4.4.1 Case 1. Lens radius is 5 kpc

This is the case where we consider the entire mass of our galaxy to be concentrated within a volume of radius smaller than the sun's distance to the center of the galaxy.

$$\Phi_{00} = 0.12 \text{x} 10^{-38}\, km^{-2}$$

$$\rho = 1.29 \text{ x } 10^{-10}\, \frac{\text{kg}}{\text{km}^3}$$

$$R_0 = 0.1545\, x\, 10^{18}\, km$$

$$R_E = 0.3616 \text{ x } 10^{18}\, km$$

Figure 4.4.1a shows the magnification of the image for the thick lens and the thin lens plotted against the impact parameter for values larger than the radius of the lens.

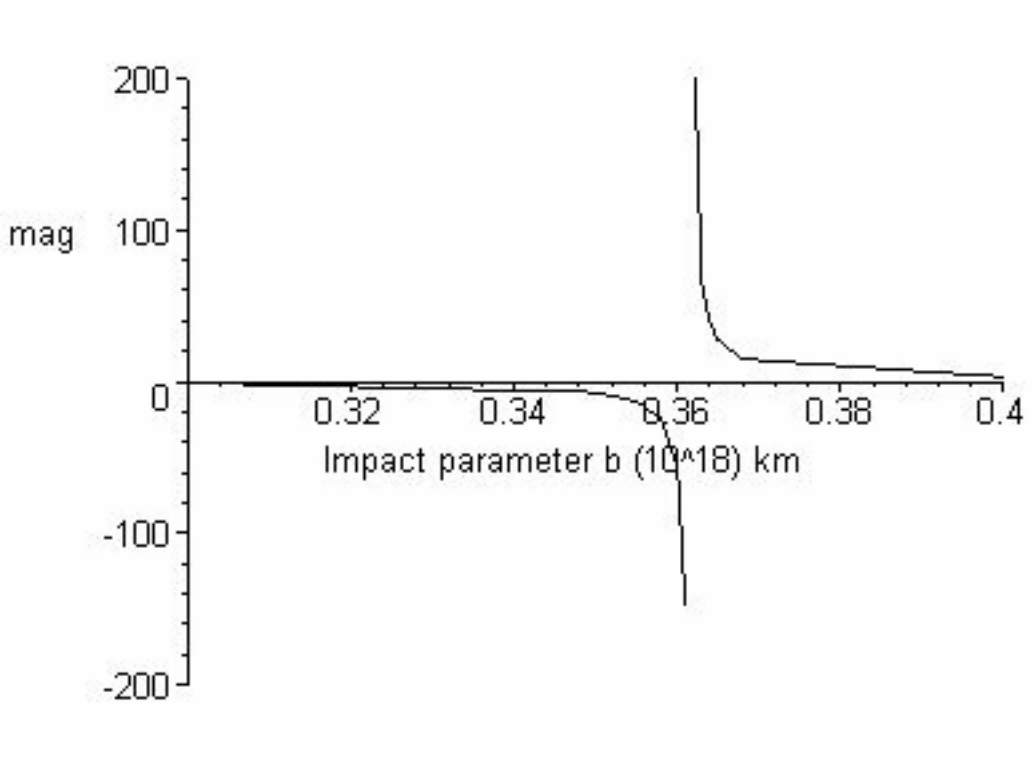

Figure 4.4.1a R=5kpc exterior region thick & thin lens mag identical at RE

The Einstein radius R_E is larger than the lens radius and is the position of the critical point outside the lens. In this case, we find that there is a second critical point that lies within the transparent lens for both the thick and the PSSTL model. The impact parameter where the second critical point is located is labeled as b_c . The magnification changes sign for both models from positive values for $b > R_E$ to negative values for $b < R_E$. In figure 4.4.1b, as the impact parameter is decreased to values less than the radius of the lens, the image in the thick lens maintains its negative sign until the value of the impact parameter is equal to $b_C = 0.1513 \text{ x } 10^{18}$ km . This is the location of the critical point inside the thick lens where the magnification is large. The magnification of the image changes sign again from

negative to positive, for values of the impact parameter smaller than b_C. In the PSSTL model the critical point inside the lens is located at $b_C = 0.1388 \text{ x } 10^{18}$ km and the magnification of the image like the thick lens changes sign too at the second critical point. In this particular case we find that there is a difference of 0.4 kpc or an angular separation of 0.02 arc second between the location of the thick and thin lens second critical point.

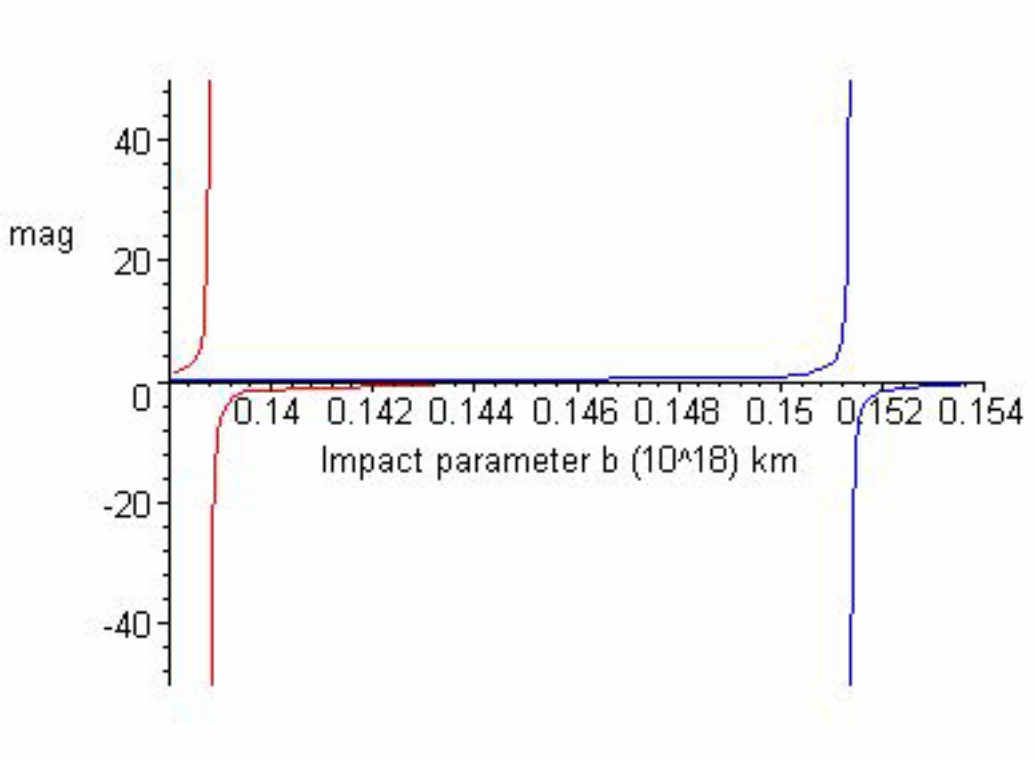

Figure 4.4.1b R=5kpc interior region thick (blue) thin (red)

4.4.2 Case 2. Lens radius is 10 kpc

This is the case when

$$\Phi_{00} = 0.15 \text{x} 10^{-39}\ km^{-2}$$

$$\rho = 1.62 \text{ x } 10^{-11}\ \frac{\text{kg}}{\text{km}^3}$$

$$R_0 = 0.309\ x\, 10^{18}\ km$$

The magnification of the thick and thin lens is plotted against the impact parameter for values outside the lens in figure 4.4.2a and for values inside the lens in figure 4.4.2b.

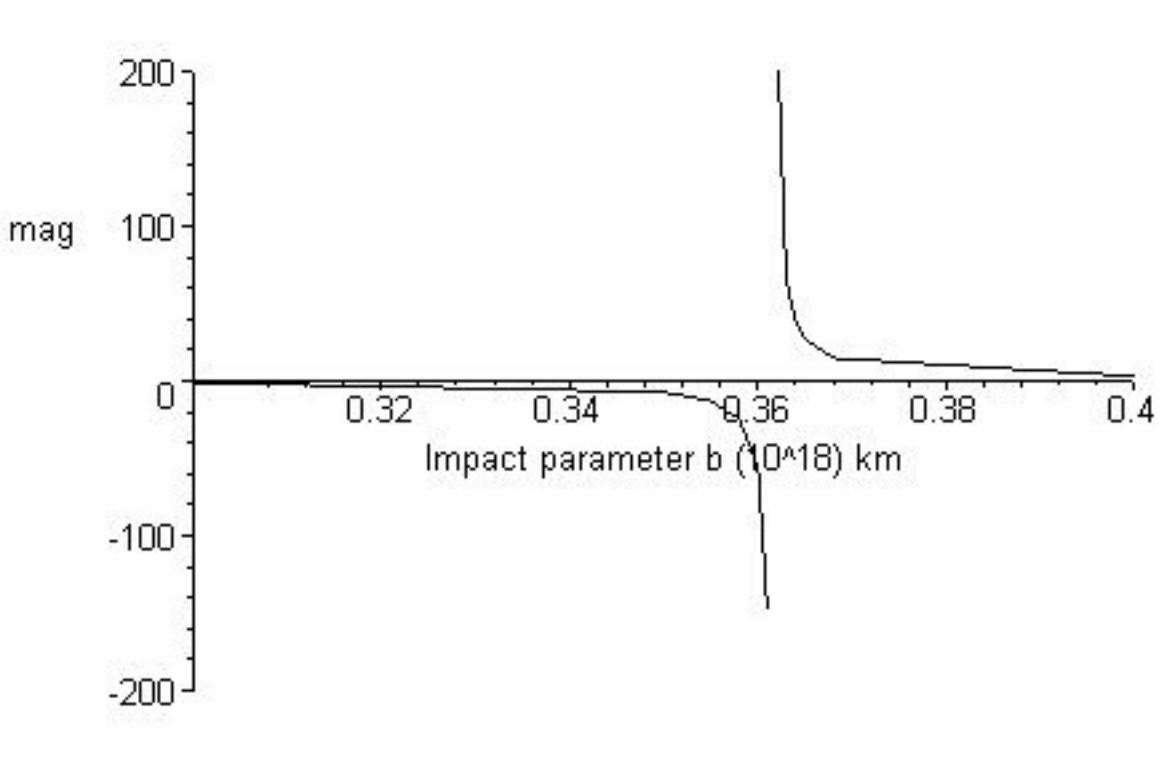

Figure 4.4.2a R=10kpc exterior region thick & thin lens mag coincides

We find a critical point at the Einstein radius which lies outside the lens. The magnification is large at R_E and again at the second critical point inside the lens at $b_C = 0.20 \text{ x } 10^{18}$ km. The PSSTL model also gives two critical points, one at R_E and the second one at b=0.23 x 10^{18} km. The image changes sign for both models at each critical point in the PSSTL and the thick lens model. The two critical points inside the lens for the thick and thin lens are separated by 1 kpc or 0.05 arc second.

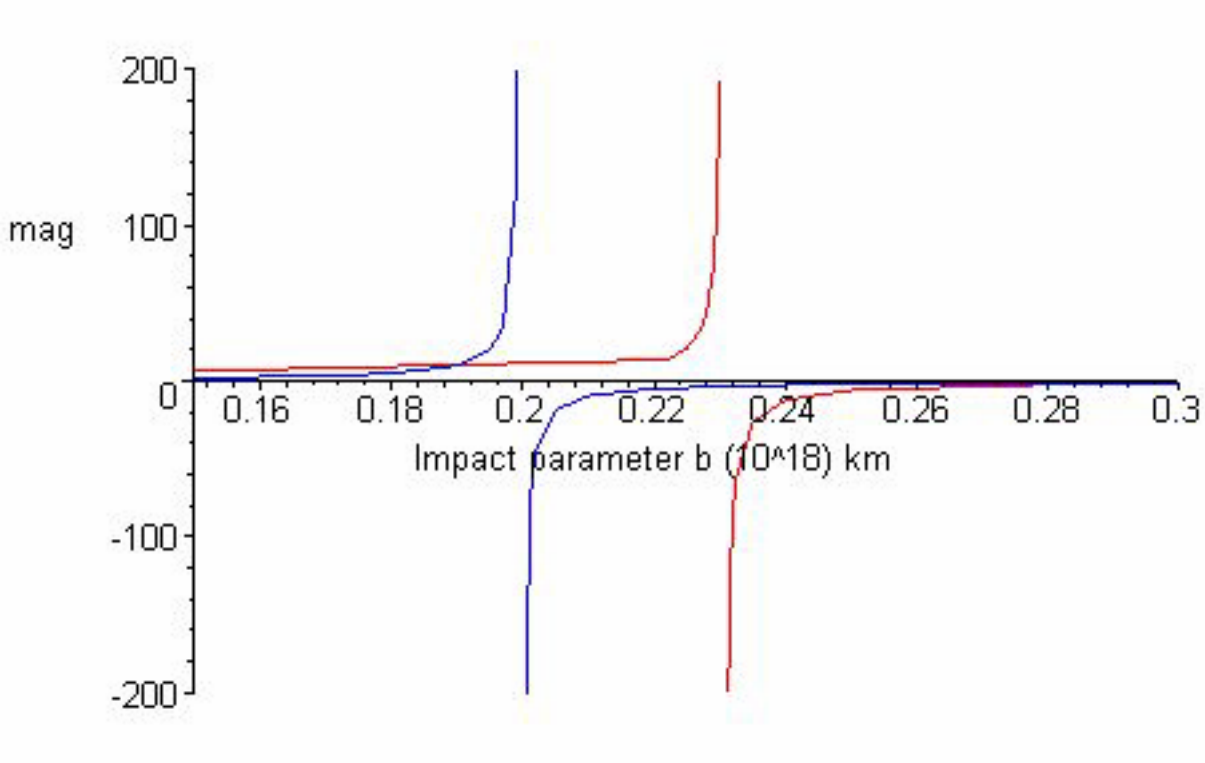

Figure 4.4.2b R=10kpc interior region thick (blue) thin (red)

4.4.3 Case 3. Lens radius is 15 kpc

This is the case that places the entire mass of our galaxy, both visible and dark matter within this radius.

$$\Phi_{00} = 0.446 \text{x} 10^{-40}\ km^{-2}$$

$$\rho = 4.80 \text{ x } 10^{-12}\ \frac{\text{kg}}{\text{km}^3}$$

$$R_0 = 0.4635\ x\, 10^{18}\ km$$

$$R_E = 0.3616 \text{ x } 10^{18}\ km$$

The magnification for both models is plotted against the impact parameter for values smaller than the lens in figure 4.4.3.

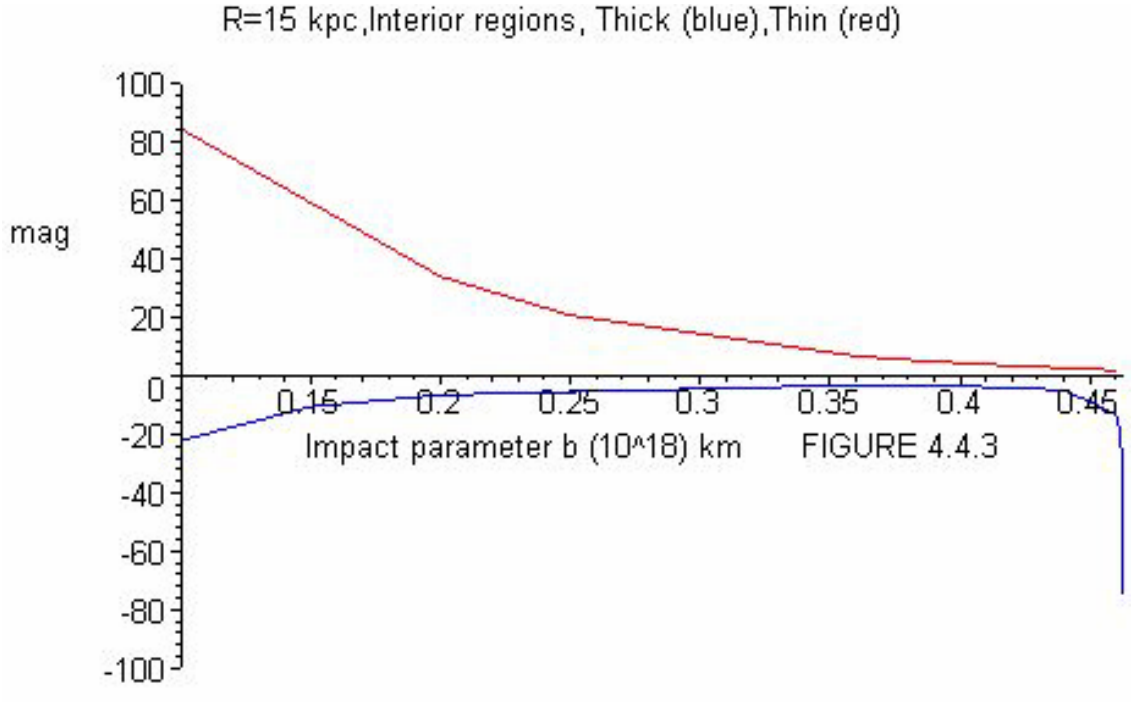

Figure 4.4.3 R=15kpc interior region thick (blue) thin (red)

In this case the Einstein radius is smaller than the radius of the lens. For the PSSTL model there is an increase in magnification of the image inside the lens but no critical points are found whereas in the thick lens model we find one critical point located at b=0.46335 x 10^{18} km almost coinciding with the radius of the lens at 0.4635 x 10^{18} km. The image magnification for the thick lens changes sign from positive to negative at b=0.4635 x 10^{18} km and then remains negative after that. The magnification in the PSSTL model shows no change in sign but increases to a large value and then decreases.

4.4.4 Case 4 Lens radius is 50 kpc

Here we assume that the dark matter in our galaxy extends to a radius much larger than the visible disk.

$$\Phi_{00} = 1.205 \text{x} 10^{-42}\ km^{-2}$$

$$\rho = 1.29 \text{ x } 10^{-13}\ \frac{\text{kg}}{\text{km}^3}$$

$$R_0 = 1.545\ x\, 10^{18}\ km$$

$$R_E = 0.3616 \text{ x } 10^{18}\ km$$

The magnification is plotted against the impact parameter in figure 4.4.4 for values of the impact parameter smaller than the lens.

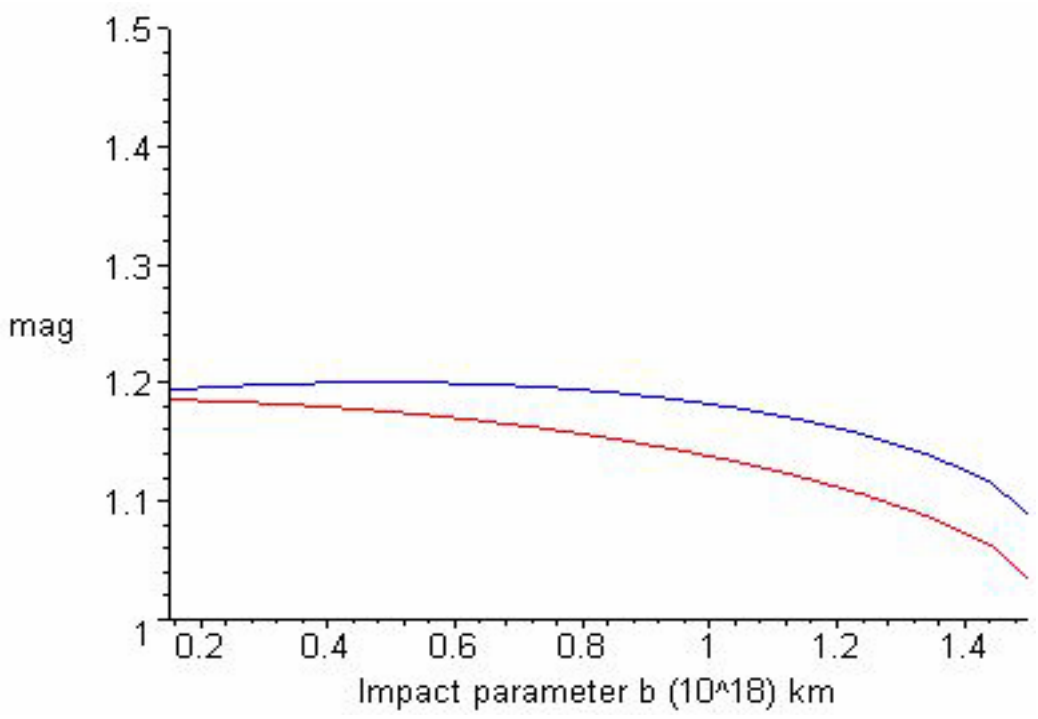

Figure 4.4.4 R=50kpc interior region thick (blue) thin (red)

The Einstein radius is located inside the lens. For this low density lens, we find that both PSSTL and the thick lens model produce no large magnification of the image inside or outside the lens.

4.5 INTERPRETATION OF RESULTS

In the thick and thin lens model we find critical points for some of the lenses, for others there are none. In order to understand the relationship between the location of critical points, parity reversal (change in sign of the magnification) and location of caustics we refer to figure 4.5.1 where the critical points and caustics are shown.

This is the case when a lens has two critical points one inside and the other outside. The latter coincides with the Einstein radius. For a spherically symmetric lens if the source is positioned on the optical axis, it is perfectly aligned with the lens and observer. The null rays impacting the lens plane at the Einstein radius form a magnified ringed image of the source.

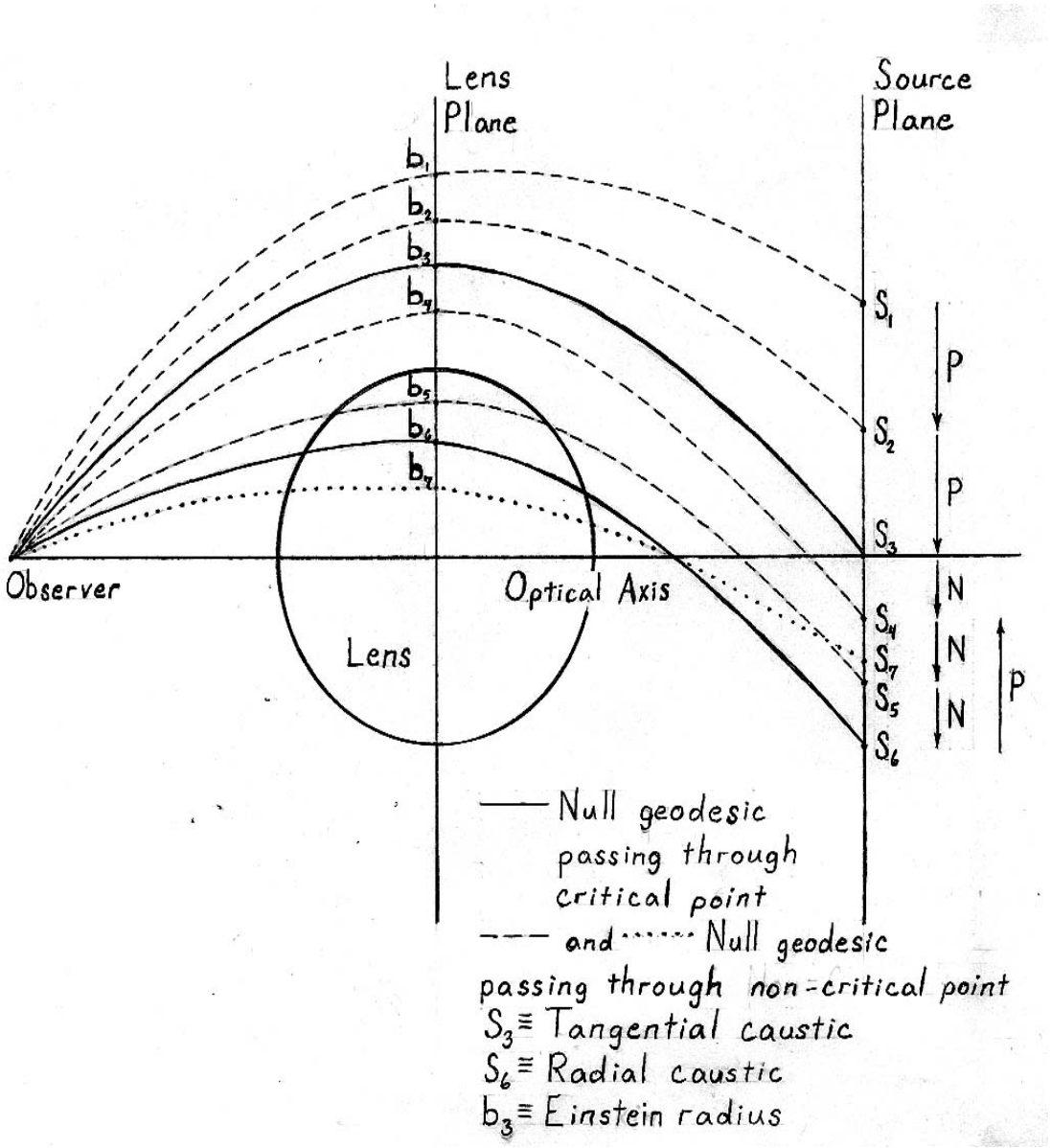

Figure 4.5.1 Lens with two critical points

The source of this ringed image is said to be located at a tangential caustic. Rays with impact parameters larger than R_E strike the source plane above the "tangential caustic" hence they have positive parity; light rays that strike the source plane below the tangential caustic reverse their parity. The null rays with impact parameters less than R_E , strike the source plane

at greater distances from the caustic. They reach a threshold point on the source plane when the rays no longer touch the source plane lower than this threshold point. This threshold point is the location of the second caustic and is known as the "radial caustic". It corresponds to the second critical point inside the lens. The light rays that impact the lens plane below the second critical point strike the source plane above the radial caustic and hence they change their parity again.

The density of the lens is critical to determine whether the light rays will bend sufficiently to form a caustic. For the very low density cases we found no critical points (see figure 4.5.2).

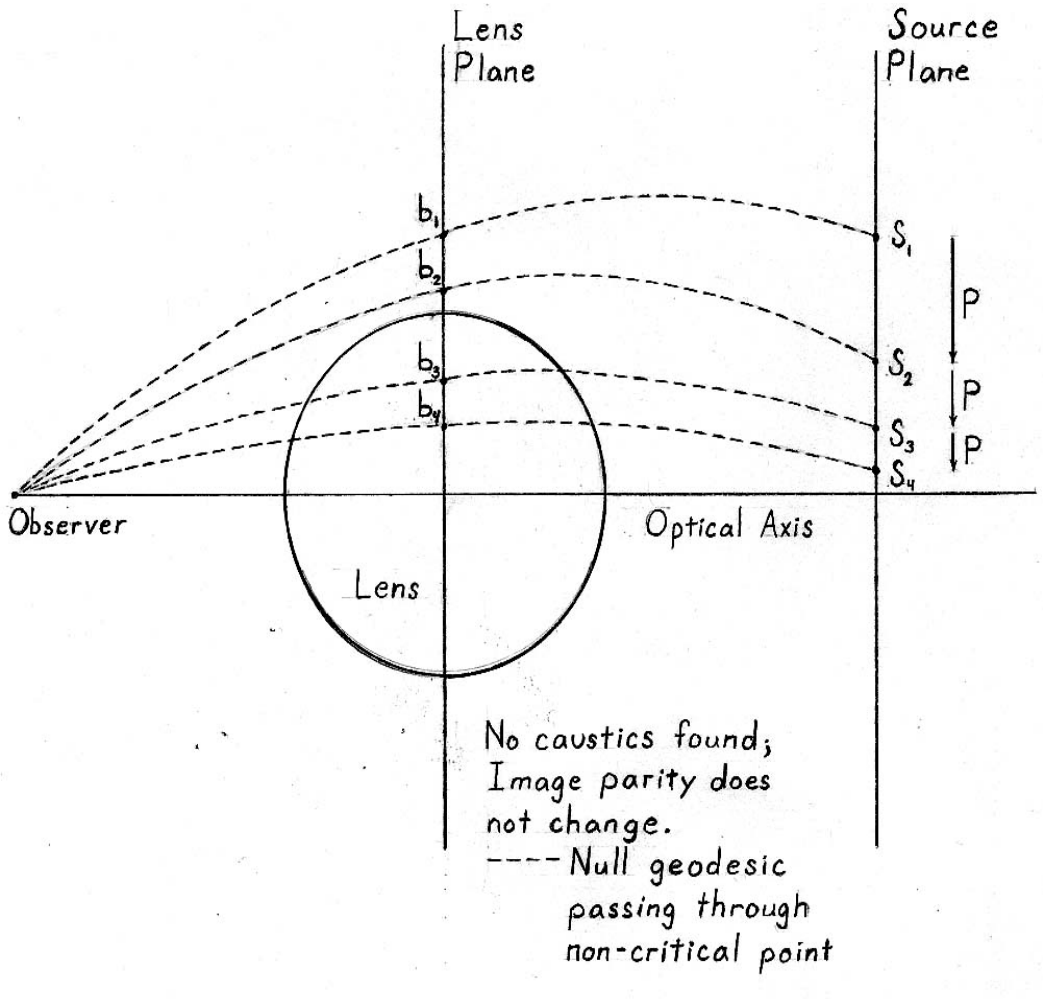

Figure 4.5.2 Lens with no critical point

The case where the dimensionless surface density is close to one, we find one critical point located inside the mass or Ricci part of the lens and lying close to the radius. In this case the tangential and the radial caustics merge (see figure 4.5.3). From these observations we can deduce that a lens with a surface density equal to the critical density will have one critical point located on the edge of the lens.

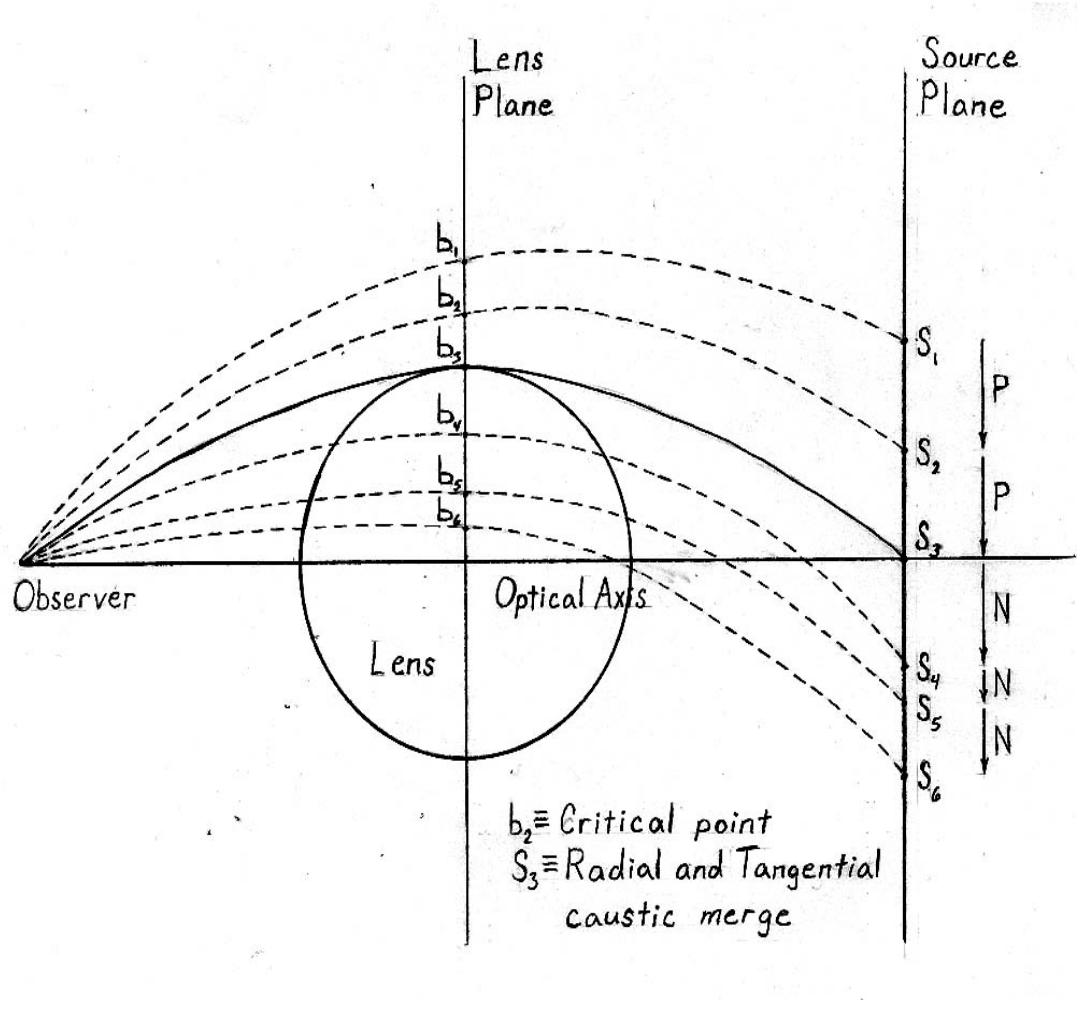

Figure 4.5.3 Lens with one critical point

In section 4.1, from equations 4.1.5-4.1.7, we examined the value of the convergence that will give a large magnification of the image of the source.

For our hypothetical lenses the convergence values were as follows:

$\kappa_{5kpc} = 8.22$, one critical point outside and one inside

$\kappa_{10kpc} = 2.05$, one critical point outside and one inside

$\kappa_{15kpc} = 0.913$, two critical points inside the lens

$\kappa_{50kpc} = 0.082$, no critical points inside or outside the lens

The 5 kpc and 10 kpc lenses have both values of $\kappa > 1$ and we find two critical points for both of them. The 50 kpc lens has a value of $\kappa < 1$ and it has no critical points. The case when the lens radius is 15 kpc we find $\kappa \approx 1$. This is where we find a discrepancy between the thick lens result and the PSSTL result. The presence of one critical point in our model with none in the PSSTL model shows that this is the correction to the thin lens model due to the thickness of the lens and it occurs close to the critical value of the convergence.

The figures in section 4.4 for the opaque lens demonstrate that for values of b larger than $R_{0,}$ the thick lens magnification is almost the same as the thin lens model. For values of b inside the lens the thick lens magnification is often quite different from the PSSTL model.

In chapter 5 we will examine an example of a possible transparent astrophysical lens.

5.0 APPLYING THE THICK LENS MODEL TO ASTROPHYSICAL LENSES

In this chapter we apply our thick lens model to simulate three types of astrophysical lenses:

(a) a galaxy cluster which is an example of a genuine transparent astrophysical lens (section 5.1)

(b) a galaxy that is like our Milky Way Galaxy (section 5.2) and

(c) a star that microlenses another star (section 5.3).

The goal in each case is to test whether the differences in the magnification of the image as determined by the thick lens model is significantly different from the thin lens model. Since we assume a spherically symmetric lens with a uniform density, which is unphysical for galaxies and galaxy clusters, it is not relevant to compare our results with observation. Instead it is important to establish the magnitude of the difference between the thick and thin lens model for future modeling applications. In the case of a star these assumptions are standard and just for curiosity we test our result with observation.

5.1 THE GALAXY CLUSTER

The astrophysical lenses that allow images of quasars or distant galaxies to be seen through the lens are clusters of galaxies. Currently, over a dozen transparent galaxy clusters have been observed. Such lenses often show multiple images inside the lensing cluster and numerous arclets encircling the outer fringes of the lens. The galaxy cluster that we modeled as our transparent lens was Abell 2218. The Abell 2218 cluster is believed to consist of about 10,000 galaxies. If we assume that the galaxies in Abell 2218 are on an average like the mass of the Milky Way Galaxy, then including the dark matter, the mass of Abell 2218 would be $M = 10^{16}\ \mathrm{M}_{\mathrm{Sun}}$. We also decided to pick distances to our source and lens different from the Abell cluster's distance. Realizing that astrophysical sources that are imaged by clusters are either quasars that lie at distances of $z > 0.5$, or they are distant galaxies that lie as far away as $z > 5.0$ we chose a source with a redshift of $z_S = 1.0$. The redshift of the Abell 2218 cluster is known to be 0.171. We chose a higher redshift for the lens, $z_L = 0.5$. Using a smaller cluster radius, and using the redshifts to determine the source and lens distances (Appendix C), the Einstein radius was found to be outside the lensing cluster. The parameters of the cluster that were used in our thick and PSSTL model, listed below, were chosen so that the Einstein radius was outside the matter region:

(i) the mass of the cluster is $M = 10^{16}\ \mathrm{M}_{\mathrm{Sun}} = 2.0 \times 10^{46}\ kg$

(ii) the radius of the cluster is $R_0 = 1\ \mathrm{Mpc} = 3.09 \times 10^{19}\ \mathrm{km}$

(iii) the Einstein radius is $R_E = 3.125 \text{ x } 10^{19} \text{ km}$

(iv) the distance to the cluster is $D_L = 4.78 \text{ x } 10^{22} \text{ km}$

(v) the distance to the source is $D_S = 9.705 \text{ x } 10^{22} \text{ km}$

(vi) the distance between the source and the lens is $D_{LS} = 4.928 \text{ x } 10^{22} \text{ km}$

(vii) the density of the cluster is $\rho = 2.02 \text{ x } 10^{-13} \frac{\text{kg}}{\text{km}^3}$

(viii) the dimensionless surface mass density of the cluster is $\kappa = \frac{\Sigma}{\Sigma_{cr}} = 2.26$

The magnification of the image is plotted against the impact parameter in Figure 5.1.1. The figure shows a change in the sign of the magnification on adjacent side of the Einstein radius. The magnification increases tremendously near the Einstein radius but it is not situated at the same location for both the thick and thin lens model. The difference in the position is 0.5 kpc = 1.56 x 10^{16} km or 0.067 arc seconds. This is small on cosmological scale but discrepancies in the Einstein radius is reflected in the mass of the lens. The ratios of the square of the Einstein radius of the thick and the thin lens gives the ratio of the thick lens mass to the thin lens mass.

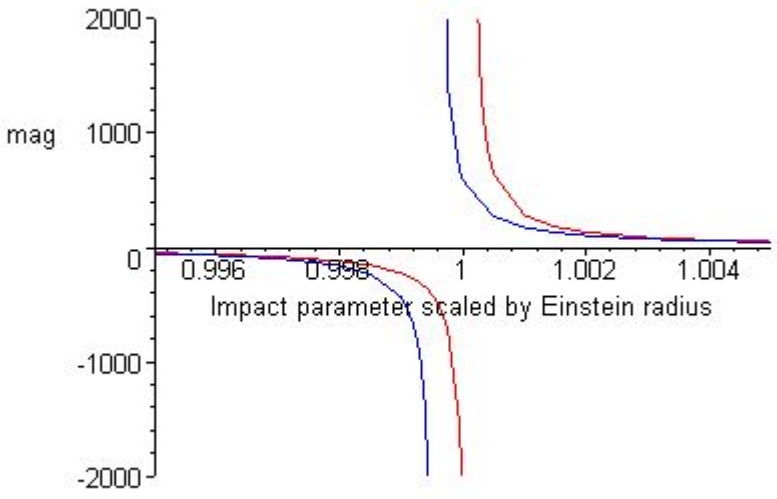

Figure 5.1.1 Exterior of Galactic Cluster, R=1Mpc, thick (blue) & thin (red)

$$\frac{R_{ET}^2}{R_{E0}^2} = \frac{M_T}{M_0} \tag{5.1.1}$$

In equation (5.1.1) the factor $\frac{4GD_L D_{LS}}{c^2 D_S}$ does not appear as it is common to both the numerator and denominator.

Substituting the values of the thick and thin lens Einstein radius in equation 5.1.1

$$\frac{R_{ET}^2}{R_{E0}^2} = \frac{(0.9995)^2}{(1.0001)^2}$$
$$\frac{M_T}{M_0} = 0.9988 \tag{5.1.2}$$

This means the difference in mass is 0.1% which is negligible considering the uncertainties in present day cluster masses.

Fore the transparent lens there is a critical point for both the thick and thin lens but the two are separated by 164 kpc or have an angular separation of 21.8 arc second.

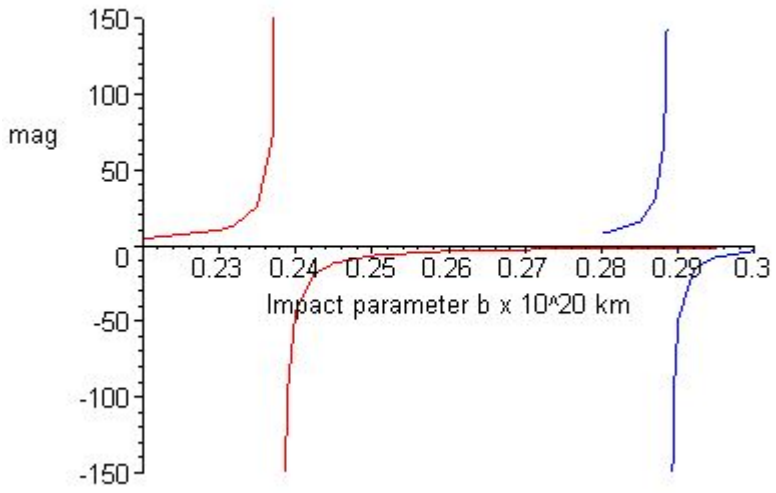

Figure 5.1.2 Interior of Galactic Cluster, R=1Mpc, thick (blue) & thin (red)

5.2 A MASSIVE MILKY WAY GALAXY

In chapter 4 we had examined four theoretical cases with the same lens mass as our Milky Way Galaxy. None of the radii chosen resembled the true size of the galaxy. Here we choose an opaque lens with a more realistic radius of the galaxy and a mass ten times greater than the actual value to include dark matter.

For this case the values of the parameters, were chosen to resemble a cosmological gravitational lensing system.

(i) the mass of the galaxy is $M = 10^{13}\ \mathrm{M}_{\mathrm{Sun}} = 2 \times 10^{43}\ kg$

(ii) the radius of the galaxy is $R_0 = 30\ \mathrm{kpc} = 0.927 \times 10^{18}\ \mathrm{km}$

(iii) the Einstein radius is $R_E = 1.1435 \times 10^{18}\ \mathrm{km}$

(iv) the distance to the galaxy is $D_L = 1346\text{Mpc} = 4.16 \text{ x } 10^{22}$ km

(v) the distance to the source is $D_S = 2867\text{Mpc} = 8.86 \text{ x } 10^{22}$ km

(vi) the distance between the source and the lens is

$$D_{LS} = 1521\text{Mpc} = 4.7 \text{ x } 10^{22} \text{ km}$$

(vii) the density of the cluster is $\rho = 2.51\text{x } 10^{-11}$ kg/km^3

The magnification of the source is plotted against the impact parameter ($b > R_0$) for both the thick and thin lens in Figure 5.2.1. We find that far from the Einstein radius the difference in magnification between the two models is negligible but close to the Einstein radius the difference is large. Figure 5.2.2 shows a plot of the ratio of the thick lens to the thin lens magnification against the impact parameter. The percentage difference can be as large as 10 to 15% in the vicinity of the Einstein radius but far away it drops to less than 0.001%.

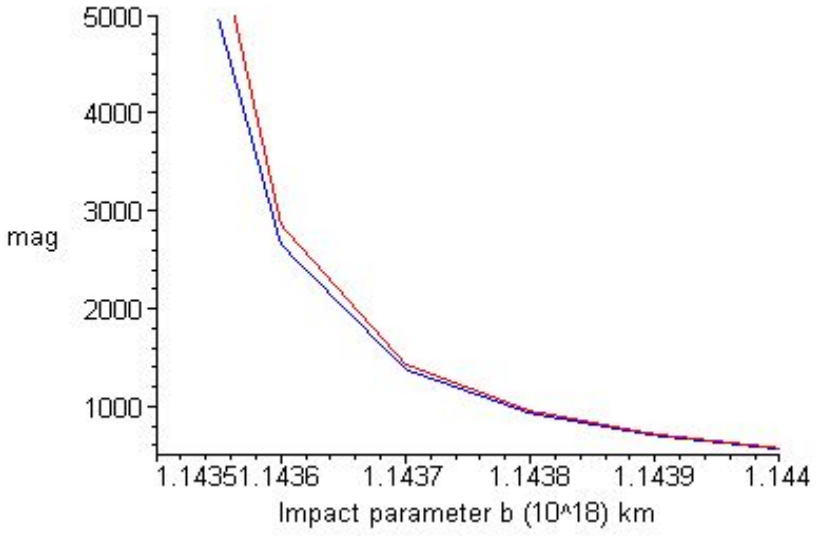

Figure 5.2.1 Exterior of 30Kpc Galaxy, thick (blue & thin (red)

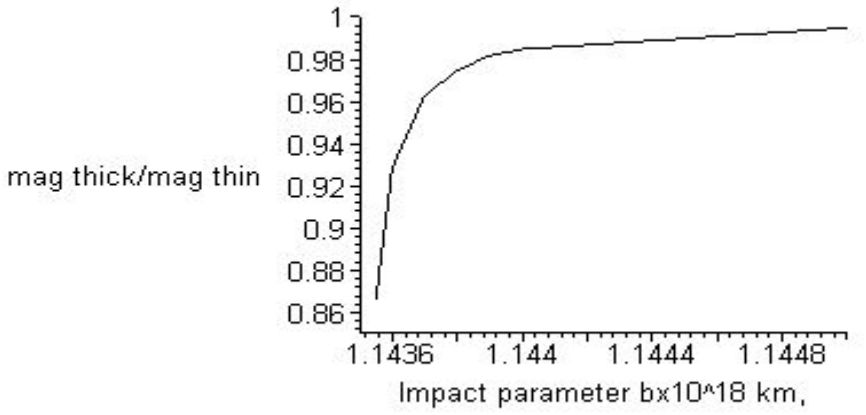

Figure 5.2.2 Ratio of thick to thin lens magnification of Galaxy

5.3 MICROLENSING DUE TO A STAR

To compare our thick lens model for the microlensing of a star with an observed microlensing event we chose the MACHO Alert 95-30 event detected by Alcock et al. (1995). The lensing star is probably a bulge star at a distance of 6.93 kpc. The source is a red giant of spectral case M4 III. Alcock et al. determined the spectral type from the spectral atlas of Turnshek et al. (1985). This implies that the radius of the star is $(61 \pm 12)\mathrm{R}_{SUN}$. From the Color Magnitude Diagram of the stars near the field of the source star, the location of the source star revealed that it lies in the galactic bulge, about 9 ± 1 kpc from the observer. The microlensing parameters that we use in our calculation are taken from Alcock et al.'s paper. Although the source is a giant

star we assume in the thick and thin lens models that it is a point source and is lensed by an opaque lens with a small radius.

As the lensing star moves across the line of sight of the red giant star a brief increase in the magnification of the source occurs. In this work we model the movement of the source across the line of sight of the lens. The closest approach of the source to the optical axis is p = 2.387 x 10^7 km in the source plane (figure 5.3.1). In the lens plane, the source appears to move across the Einstein ring with an impact parameter given by p. The displacement of the source $\vec{\eta}$ from the optic axis is determined in the following manner:

$$\eta = (p^2 + v^2 t^2)^{1/2} \qquad 5.3.1$$

where v = 193 km/s is the relative velocity of the source with respect to the lens. The time t is measured in days starting with the time when the source is closest to the optical axis as the initial time. From the Einstein radius,

$$R_E = 4.42\, x\, 10^8\, km$$

and the lensing distances,

$$D_S = 9kpc = 2.78x10^{17}\, km$$
$$D_L = 6.93kpc = 2.14x10^{17}\, km$$

the mass of the lens is determined to be $M_{Lens} = 0.67 M_{SUN}$

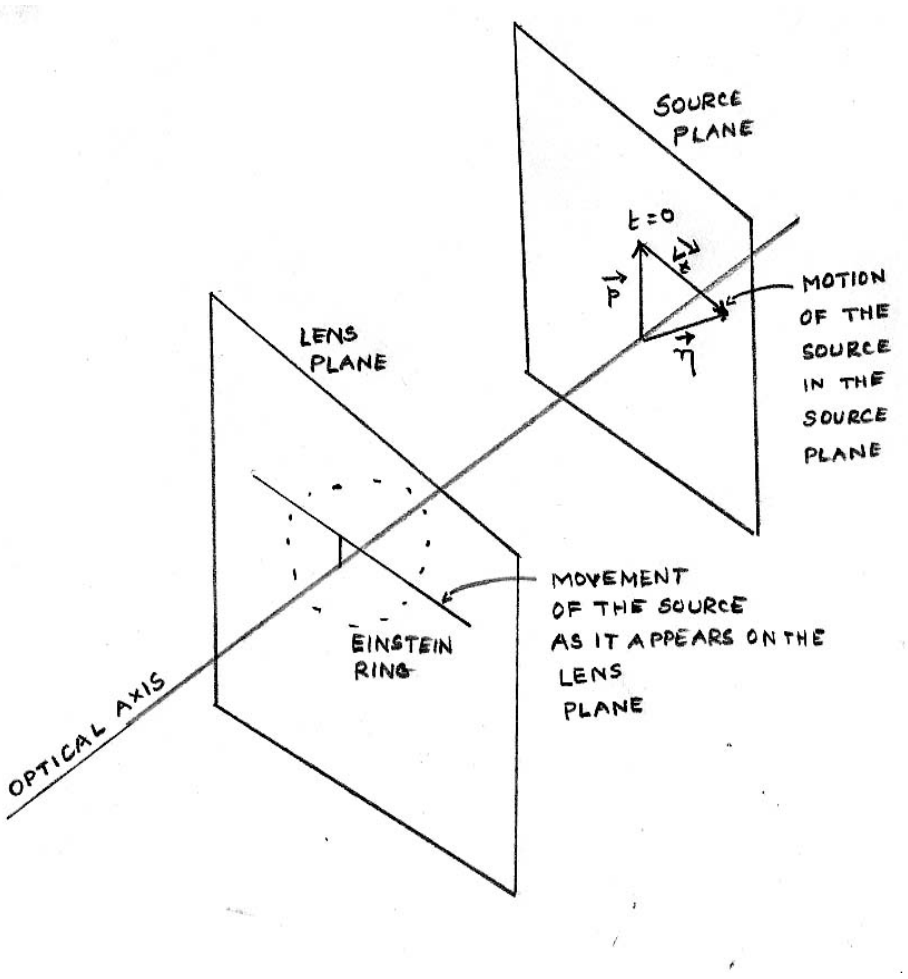

Figure 5.3.1 Projection of source's motion on lens plane

To find the impact parameter $\vec{\xi}$, the thin lens equation is used,

$$\frac{D_L}{D_S}\vec{\eta} = \vec{\xi} - \frac{R_E^2}{\vec{\xi}} \qquad 5.3.2$$

The spherical symmetry of the lens makes the above equation a quadratic equation in the scalar ξ:

$$\xi^2 - (\frac{D_L \eta}{D_S})\xi - R_E^2 = 0 \qquad 5.3.4$$

The roots of this equation, gives the two impact parameters in the lens plane, where the image is located. One image is found inside the Einstein ring the other outside. The combined magnification of the two images gives the total observed magnification of the source. The magnification for each of the image is determined from the thick lens model and the thin lens model. To find the magnification in the thick lens model the null geodesic is taken to pass through the constant curvature matrix region having a width given by:

$$w = 2\sqrt{(4R_E^2 - b^2)} \qquad 5.3.5$$

For each value of the source position η the combined magnification of the two images in the thick lens model is

$$\mu_T = |\mu_{1T}| + |\mu_{2T}| \qquad 5.3.6$$

and in the thin lens model is

$$\mu_0 = |\mu_{10}| + |\mu_{20}| \qquad 5.3.7$$

The thick lens magnification for each of the two impact parameters ξ_1 and ξ_2 corresponding to a particular source position is given by

$$\mu_{jT} = \frac{D_S^2}{\det \overline{X}_{III}(\xi_j)}, \ \mathrm{j} = 1,2 \qquad 5.3.8$$

The denominator in equation (5.3.8) is the determinant of the solution to the geodesic deviation equation at the source. The numerator is the square of the distance to the source.

The same impact parameters were used to determine the magnification of the source in the thin lens model. We now show how the expression for the traditional thin lens magnification can be written in a simple form.

For a point source the thin lens magnification is given by equation 2.2.5 found directly from Schneider et al. as

$$\mu_{\pm} = \frac{u^2+2}{2u(u^2+4)^{1/2}} \pm \frac{1}{2}$$
$$\mu_{+} = \mu_{01};\ \mu\_ = \mu_{02}$$
$$u = \frac{\eta D_L}{D_S R_E} \qquad 5.3.9$$

Using η from equation (5.3.4), u becomes

$$u = \frac{\xi^2 - R_E^2}{\xi} \qquad 5.3.10$$

Substituting this value of u into the first equation of (5.3.9)

$$\mu_{+} = \frac{\xi^4 - 2\xi^2 R_E^2 + R_E^4 + 2\xi^2 R_E^2}{2(\xi^2 - R_E^2)\{(\xi^2 - R_E^2)^2 + 4\xi^2 R_E^2\}^{1/2}} + \frac{1}{2}$$
$$= \frac{\xi^4 + R_E^4}{2(\xi^2 - R_E^2)(\xi^2 + R_E^2)} + \frac{1}{2} \qquad 5.3.9$$
$$= \frac{\xi^4}{\xi^4 - R_E^4}$$

Using this equation we found the time dependent magnification in the thin lens model for the microlensed star.

From equations (5.3.6) and (5.3.7) the magnification of the thick and thin lens are plotted against the time. Figure (5.3.2) shows the light curves for the two models. Figure 5.3.3 is the light curve of the observed event.

The peak magnification between the thin and thick lens differs by 0.8, the thin lens being higher than the thick lens. We compare these two light curves with the observed light curve given in Alcock et al.'s paper (1997). The observed peak magnification lies between the thick and thin lens model. We also plot the graph of the ratio of the thick and thin lens magnification.

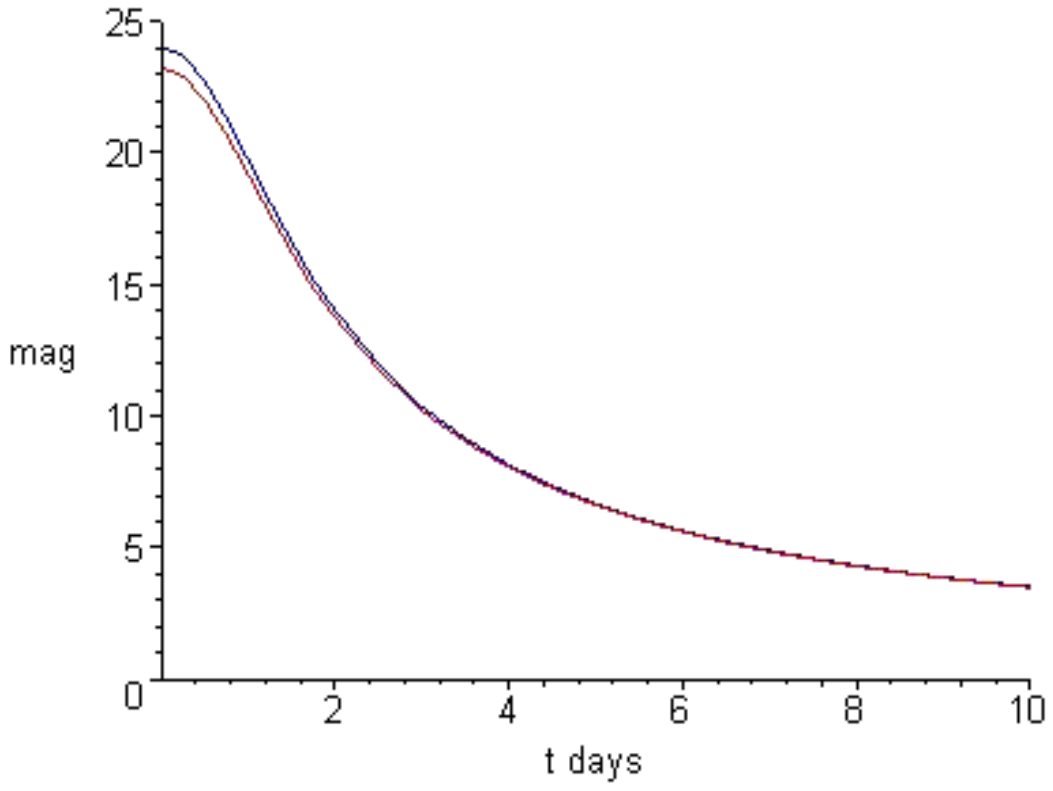

Figure 5.3.2 Light curve of MACHO Alert 95-30, thin lens (blue) & thick lens (red)

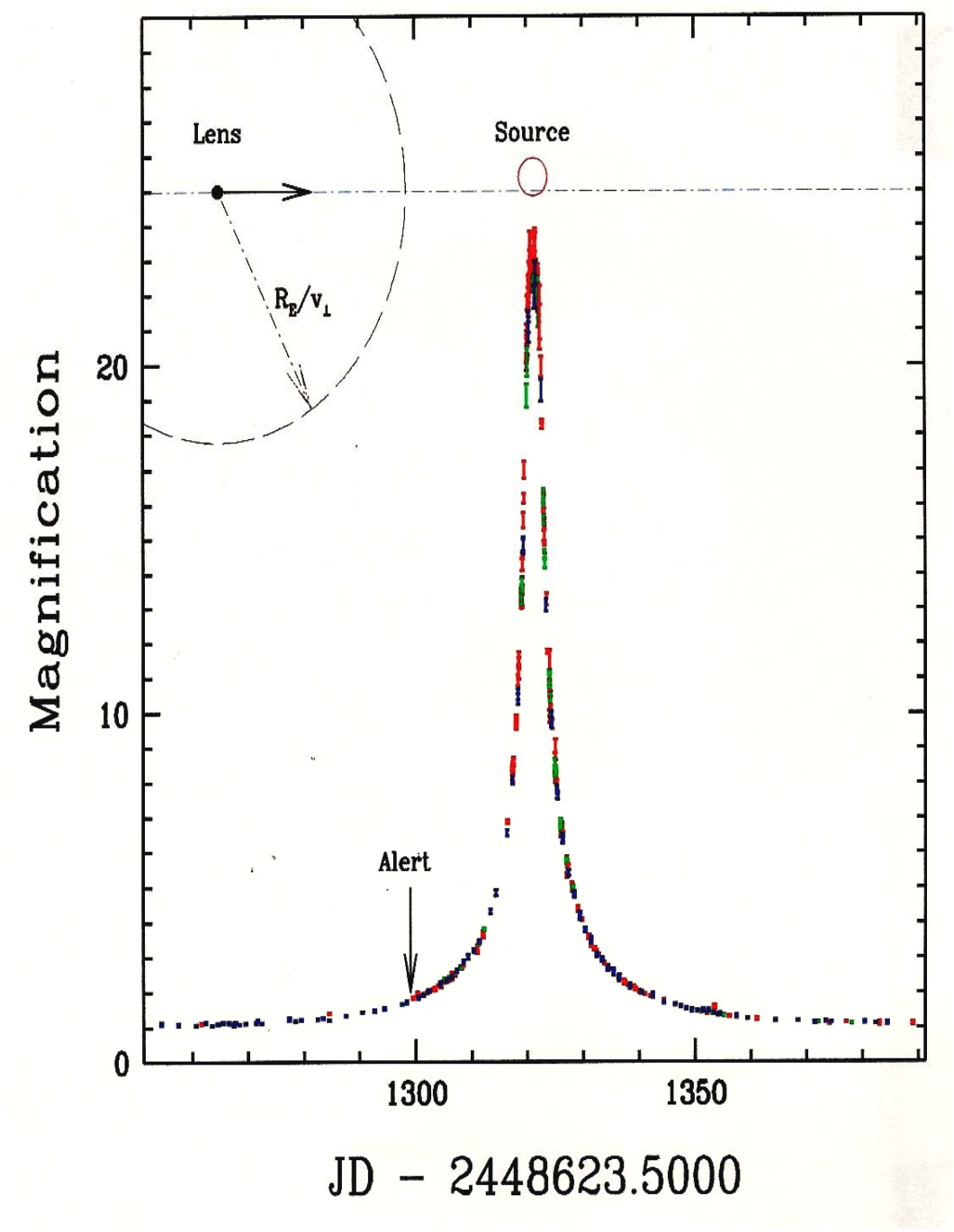

Figure 5.3.3 Light curve of MACHO Alert 95-30, Alcock et al., 1995

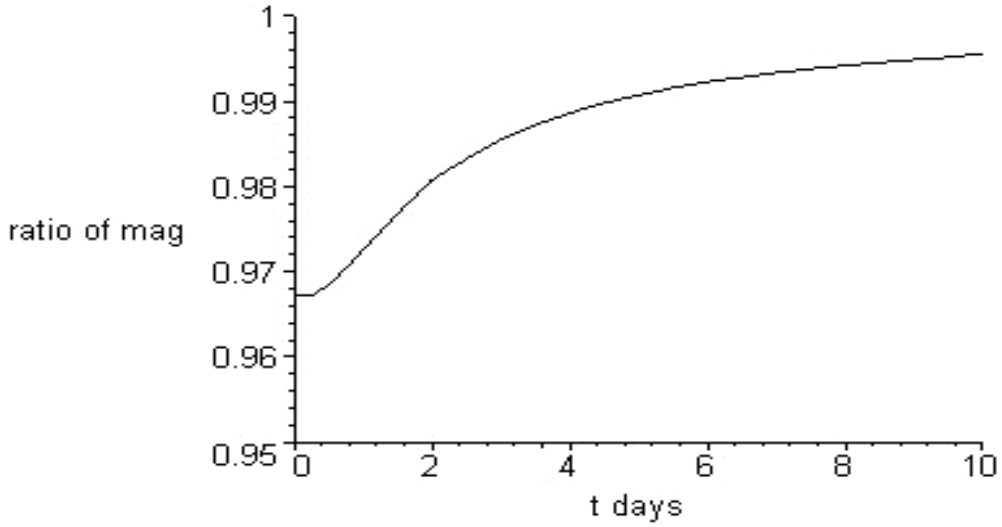

Figure 5.3.4 Ratio of thick to thin lens magnification, MACHO Alert 95-30

6.0 CONCLUSION

In this thesis we developed a model for gravitational lensing that we referred to as the thick lens model. This model is based on the idea that perhaps the standard, almost universally used, thin lens calculations could be in error under certain circumstances and that perhaps the use of a thick lens could sometimes correct those errors. For the sake of model building, we have assumed that our lens is spherically symmetric hence the Schwarzschild metric yields an appropriate space-time description. The idea is to compare the magnifications from both the thick and the thin lens models and, if differences do show up, to compare them with observations.

It did turn out that the difference in magnification of a gravitationally lensed source, determined by the thick lens and the universally accepted thin lens approximation, and does in fact appear to be quite small in most circumstances. But there were real differences in special cases. Both these results could be seen from the Taylor series expansion in the width of the thick lens in the limit of the width approaching zero and from the detailed individual comparisons.

There were, as we mentioned, scenarios where the difference could be significant and hence require special attention. We found the largest difference in magnification between the two models for the case when the lens was transparent and the light rays traversed the interior of the lens.

One of the questions about thick lenses that were of primary concern in this work was determining the effect of changes in the width of the region of constant Weyl curvature on the

magnification. Applying a variety of widths to lenses of different sizes we found that slow but appreciable changes in width has only, in general, a small effect on the magnification of the source in the thick lens. This excludes the choice of extremely large widths that gave us unphysical results.

There were three scenarios in the vacuum region where we did find a real difference between the thick and thin lens models. These were for lenses that simulated a galactic cluster, a galaxy and a star microlensing another star.

We first summarize the results from the galaxy cluster.

Though we treat the galactic cluster as transparent, we first discuss the vacuum region. Our thick lens model when applied to the cluster showed appreciable variation in magnification between the thick and thin lens models near the Einstein radius. It was apparent that the large difference in magnification near the Einstein radius is due to the fact that the Einstein radius does not coincide in the two models. The difference in the two Einstein radii was 0.5 kpc (0.067 arc second). This difference is certainly negligible in cosmological terms. But the Einstein radius is important because it is an observable feature among large lenses in the cosmos. The angular diameter of the Einstein ring constrains the mass of the lens and can be determined if the distances to the lens and the source are known. A 0.5 kpc difference in the ring diameter implies that the mass of the lens calculated in the two models differ by 0.1 %. Clusters of galaxies are so massive that a 0.1 % difference can be a major error. Although mass determination of clusters to this level of precision is unheard of now but it could be a possibility in the distant future. The results for the magnification of the source for this transparent lens in the non-vacuum region will be summarized later.

The second example of a cosmic lens was a galaxy similar to our Milky Way Galaxy, which is non-transparent. We chose a mass ten times larger than the accepted value and a radius twice that of the visible disk to take account of the dark matter. Here we found the difference in magnification between the thick and thin lens models to gradually increase around the Einstein radius. Far from the Einstein ring the percentage difference in magnification was less than 0.001 %. But the difference increased and was as high as 10-15% near the Einstein radius.

Our third astrophysical lens is a non-transparent star. For this particular case we applied our model to an actual observed microlensing event (MACHO-Alert 95-30). Here a star in the bulge of our galaxy had microlensed another giant star in the bulge and the light curve of this event was observed by astronomers. Using the actual observable parameters to model this lens we determined the light curve for the thick and thin lens models. The largest disparity in magnification among the two models was found for this case. For the MACHO-Alert 95-30 event, the peak magnification differs by 3 percent between the thin and thick lens. Some would argue that this is too small a discrepancy to be observable. Presently, fluxes of stars are observable to 0.005 of a magnitude and microlensing events with extreme precision are being undertaken. This small deviation of today could in future translate to an observationally significant difference. Both the models predicted a light curve that was comparable with the observed light curve and became indistinguishable far from the closest approach of the lens and source. The observed peak magnification was found to have a value less than the thin but more than the thick lens model. In fact many claim this source should be considered an extended source since it is a red giant, but both the thin and thick lens model of a point source did a good job of fitting the light curve.

One of the objectives of this study was to model transparent lenses regardless of their feasibility. We wanted to test the relationship between the density of the lens and the location of the critical points and caustics. In order to compare our model for the interior regions of the transparent lens with the thin lens we chose the PSSTL model. This enabled us to compare the thick lens source magnification with the PSSTL model when the null geodesics passed through the lens. Recapitulating our model, in the case of a transparent lens when the light rays were outside the lens, the thick lens magnification was compared with the standard thin lens approximation; when the light rays passed through the lens the thick lens magnification was compared with the magnification obtained by the PSSTL model.

We now review the results of the transparent non-realistic lenses and the plausible transparent lens, i.e., the galaxy cluster.

The four theoretical lenses that we examined showed that the light rays passing through the transparent lens would produce a very large magnification of the source when the density of the lens was close to the critical density. The high density lenses would show large magnification for two pairs of impact parameters; one at the Einstein radius and other inside the lens on either side of the optical axis. The image changed parity whenever the impact parameter crossed a critical point. These observations were true for thick and thin lens.

The location of the interior critical point is a function of the critical density. As the surface density approached the critical density value, the two critical points, one inside and the other outside decreased their separation. This observation was not always true for the PSSTL model.

We believe that when the surface density is exactly equal to the critical density then the Einstein radius coincides with the radius of the lens.

This latter case was not tested but we did apply our model to a lens with a surface density close to the critical density. This lens had both the critical points inside the lens. In this case the Einstein radius was located within the lens. What physical significance an interior Einstein radius can play is not known but we did observed a large increase in magnification at this impact parameter where our critical point was located. However the spherically symmetric thin lens did not show a large magnification at the Einstein radius. In this case the PSSTL model's magnification increased substantially and reached a maximum value over 100 but no where near the Einstein radius.

For the 5 kpc and 10 kpc radii lenses the location of the critical points inside the lens differed considerably between the thick and the PSSTL model. The location of the Einstein radius, in both cases, was situated outside the lens and was the same as the thin lens approximation. The difference in magnification was less than a hundredth of that of the thick lens. For the very low density lens of 50 kpc the two models showed little difference in magnification inside and outside.

In all the lenses and in both the models the magnification would decrease as the impact parameter approached the center of the lens. Our analysis was terminated for impact parameters close to the Schwarzschild radius where the linear approximation breaks down.

We also showed geometrically the location of the tangential and radial caustics. When the null rays strike the source plane and cross or touch the caustic it changes sign and hence change the parity of the lens. When the source is located on the optical axis it was a tangential caustic. This is the basis of the Einstein ring where rays from every point on the circumference of the ring would converge to the tangential caustic. If the location of the source anywhere else

gave rise to a caustic then the critical point was located inside the lens. The distance to the source and lens also affected whether a lens possessed a caustic.

The motivation for doing this work was based on astrophysical observations that showed there was a discrepancy between theoretical calculation and observations for certain complicated lens configuration of the magnification of a source with multiple images as observed by optical telescopes and radio telescopes. One of the suggestions that have been made was: could considerable dust in the lensing galaxy have anomalous effect on the magnification of the source as observed by different telescopes. With our transparent lens we might be able to address the issue of the discrepancy. Our idea was to raise the possibility that the thickness of the lens could sort this issue. Another problem in astronomy is the determination of the dark matter content in galaxies and cluster of galaxies. We believe the thick lens model has the potential to determine to some extent the amount of dark matter associated with a gravitational lens. The more recent claim by astronomers of substructure in the lens which leads also to observed magnification discrepancies can be examined with our transparent thick lens.

6.1 FUTURE GOAL

The thick lens model that is developed here has limited application in astrophysics. To make our model more realistic the next step is to make a pyramid like model with varying Ricci and Weyl tensors that would represent varying density and strength of the space-time curvature, respectively. The idea is to model the variation in density that is normal in cosmic lenses. The Weyl tensor that is assumed to have a uniform strength both inside and outside the lens in this thesis would be changed with different heights reflecting variation in strength. Similarly, the

Ricci would have different heights representing the variation in density of the halo, the disk and the bulge if we are using the galaxy as a lens. We illustrate our pyramid model in figure 6.1

Recent observations of the Einstein cross appearing within the bulge of the galaxy would be an interesting cosmic lens to study with our thick lens model but modified to use regions of at least two different mass densities.

Presently, our thick lens model probably has the greatest application in microlensing events. Since several groups of astrophysicists are involved in searching for microlensing events, we are interested in the possibility of applying our model to these events.

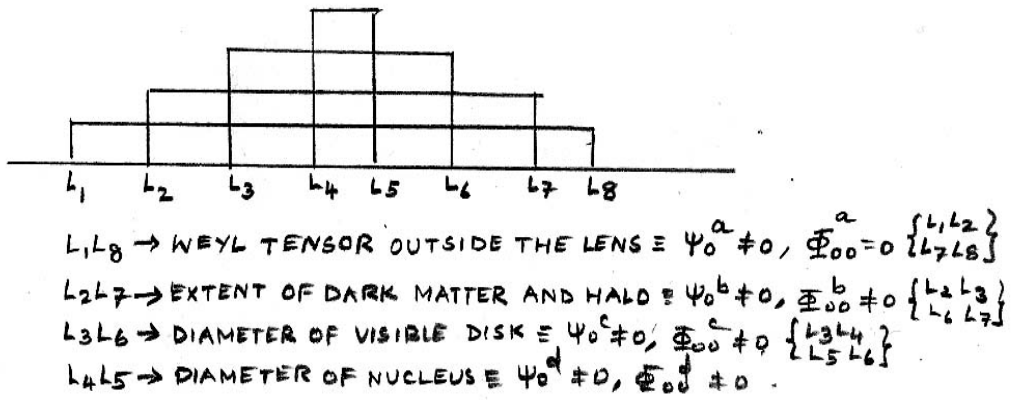

Figure 6.1 Pyramid Model of Milky Way Galaxy

We would also like to explore more comprehensively the relationship between the positions of the critical points inside the lens with the critical density and the location of the caustics.

APPENDIX A

TRANSFORMATION OF WEYL TENSOR

For a spherically symmetric mass, the space-time exterior to it can be described by the Schwarzschild solution. The metric in spherical polar coordinates is given by

$$ds^2 = (1-\frac{2m}{r})dt^2 - \frac{dr^2}{(1-2m/r)} - r^2(d\theta^2 + \sin^2\theta d\phi^2) \qquad \text{A1}$$

Here, $m = GM/c^2$, where M is the mass of the body in regular units and m is the mass of the body in geometrical units, such that m/r is dimensionless. Equation A1 is valid for r > R, where R is the radius of the spherical mass.

The Schwarzschild metric in terms of the null tetrad is given by

$$ds^2 = \eta_{ab}dx^a dx^b - \frac{2m}{r}l_a l_b dx^a dx^b$$

The components of the Weyl tensor in the null tetrad formalism is given by (Newman and Penrose, 1962)

$$\Psi_0 = -C_{abcd} l^a m^b l^c m^d$$
$$\Psi_1 = -C_{abcd} l^a n^b l^c m^d$$
$$\Psi_2 = -\frac{1}{2} C_{abcd} (l^a n^b m^l n^d + l^a n^b m^c \overline{m}^d)$$
$$\Psi_3 = C_{abcd} l^a n^b n^c \overline{m}^d$$
$$\Psi_4 = -C_{abcd} n^a \overline{m}^b n^c \overline{m}^d$$

For the Schwarzschild metric, Newman & Todd (1980) and Janis & Newman (1965) had shown that these components reduce to only one non-zero component:

$$\psi_2 = \frac{m}{r^3}$$

Therefore taking $m = a_0$

$$\psi_0 = 0,\ \psi_1 = 0,\ \psi_2 = \frac{a_0}{r^3},\ \psi_3 = 0,\ \psi_4 = 0$$

But this component depends on the radial distance r from the center of the lens. We are interested in a coordinate transformation from the radial to the cartesian coordinate z, where the z axis lies along the line of sight of the observer but is measured from the center of the lens.

Following Janis and Newman (1965), we do a rotation around l:

$$\psi_0^* = \psi_0 = 0;$$
$$\psi_1^* = \psi_1 + \bar{a}\,\psi_0 = 0;$$
$$\psi_2^* = \psi_2 + 2\bar{a}\,\psi_1 + \bar{a}^2\psi = \frac{a_0}{r^3};$$
$$\psi_3^* = \psi_3 + 3\bar{a}\,\psi_2 + 3\bar{a}^2\psi_1 + \bar{a}^3\psi_0 = \frac{3\bar{a}a_0}{r^3};$$
$$\psi_4^* = \psi_4 + 4\bar{a}\,\psi_3 + 6\bar{a}^2\psi_2 + 4\bar{a}^3\psi_1 + \bar{a}^4\psi_0 = \frac{6\bar{a}^2 a_0}{r}$$

Then a Lorentz transformation:

$$\psi_0^+ = \lambda^2 e^{2i\phi}\psi_0^* = 0$$
$$\psi_1^+ = \lambda e^{i\phi}\psi_1^* = 0$$
$$\psi_2^+ = \psi_2^* = \frac{a_0}{r^3}$$
$$\psi_3^+ = \frac{e^{-i\phi}}{\lambda}\psi_3^* = 3\bar{a}a_0\,\frac{e^{-i\phi}}{\lambda r^3}$$
$$\psi_4^+ = \frac{e^{-2i\phi}}{\lambda^2}\psi_4^* = 6\bar{a}^2 a_0\,\frac{e^{-2i\phi}}{\lambda^2 r^3}$$

Finally a rotation about n gives,

$$\hat{\psi}_0 = \psi_0^+ + 4b\,\psi_1^+ + 6b^2\psi_2^+ + 4b^3\psi_3^+ + b^4\psi_4^+$$
$$= \frac{6\mathrm{b}^2 a_0}{r^3} + \frac{12b^3 e^{-i\phi}\bar{a}a_0}{\lambda r^3} + \frac{6b^4 e^{-2i\phi}\bar{a}^2 a_0}{\lambda^2 r^3} \qquad \text{A1}$$

$$\hat{\psi}_0 = \frac{6\bar{\zeta}^2 \psi_2}{(1+\zeta\bar{\zeta})^2}$$

Null rotation around l^μ gives,

$$l^{*\mu} = l^\mu$$

$$m^{*\mu} = m^\mu + a l^\mu$$

$$n^{*\mu} = n^\mu + a\bar{m}^\mu + \bar{a} m^\mu + a\bar{a} l^\mu$$

Lorentz transformation in the l^μ, n^μ plane and rotation in $m^\mu, \bar{m}^\mu$ gives,

$$l^{+\mu} = \lambda l^{*\mu} = \lambda l^\mu$$

$$n^{+\mu} = \lambda^{-1} n^{*\mu} = \lambda^{-1}(n^\mu + a\bar{m}^\mu + \bar{a} m^\mu + a\bar{a} l^\mu$$

$$m^{+\mu} = e^{i\phi} m^{*\mu} = e^{i\phi}(m^\mu + a l^\mu)$$

$$\bar{m}^{+\mu} = e^{-i\phi} \bar{m}^{*\mu} = e^{-i\phi}(\bar{m}^\mu + \bar{a}\bar{l}^\mu)$$

Null rotation around n^μ

$$\begin{aligned}
\hat{l}^\mu &= l^{+\mu} + b\bar{m}^{+\mu} + \bar{b} m^{+\mu} + b\bar{b} n^{+\mu} \\
&= \lambda l^\mu + b e^{-i\phi}(\bar{m}^\mu + \bar{a}\bar{l}^\mu) + \bar{b} e^{i\phi}(m^\mu + a l^\mu) \\
&= \mathrm{b}\bar{\mathrm{b}}\lambda^{-1}(n^\mu + a\bar{m}^\mu + \bar{a} m^\mu + a\bar{a} l^\mu)
\end{aligned}$$

$$\hat{n}^\mu = n^{+\mu} = \lambda^{-1}\{n^\mu + a\bar{m}^\mu + a\bar{a} l^\mu)$$

$$\hat{m}^\mu = m^{+\mu} + b n^{+\mu}$$

$$= \mathrm{e}^{\mathrm{i}\phi}(m^\mu + a l^\mu) + \frac{b}{\lambda}(n^\mu + a\bar{m} + \bar{a} m^\mu + a\bar{a} l^\mu)$$

A2

Equating $l^\mu, m^\mu, \overline{m}^\mu, n^\mu$ in terms of the stereographic coordinates

$$l^\mu = [1,\ \frac{\varsigma+\bar{\varsigma}}{1+\zeta\bar{\zeta}},\ \frac{i(\bar{\varsigma}-\varsigma)}{1+\zeta\bar{\zeta}}\ ,\frac{\varsigma\bar{\varsigma}-1}{1+\zeta\bar{\zeta}}]$$

$$n^\mu = \frac{1}{2}[1,\ \frac{-(\varsigma+\bar{\varsigma})}{1+\zeta\bar{\zeta}},\ \frac{-i(\bar{\varsigma}-\varsigma)}{1+\zeta\bar{\zeta}}\ ,\frac{-(\varsigma\bar{\varsigma}-1)}{1+\zeta\bar{\zeta}}]$$

$$m^\mu = \frac{1}{\sqrt{2}}[0,\ \frac{1-\bar{\varsigma}^2}{1+\zeta\bar{\zeta}},\ -\frac{i(1+\bar{\varsigma}^2)}{1+\zeta\bar{\zeta}}\ ,\frac{2\bar{\varsigma}}{1+\zeta\bar{\zeta}}]$$

$$\overline{m}^\mu = \frac{1}{\sqrt{2}}[0,\ \frac{1-\varsigma^2}{1+\zeta\bar{\zeta}},\ \frac{i(1+\varsigma^2)}{1+\zeta\bar{\zeta}}\ ,\frac{2\varsigma}{1+\zeta\bar{\zeta}}]$$

with the null tetrads along the line of sight,

$$\hat{l}^\mu = (1,0,0,1)$$

$$\hat{n}^\mu = \frac{1}{2}(1,0,0,-1)$$

$$\hat{m}^\mu = \frac{1}{\sqrt{2}}(0,1,i,0)$$

$$\hat{\overline{m}}^\mu = \frac{1}{\sqrt{2}}(0,1,-i,0)$$

and solving for $a, \overline{a}, b, \lambda$ we have,

$$\hat{\psi}_0 = \frac{12\bar{\zeta}^2\psi_2}{(1+\zeta\bar{\zeta})^2} = \frac{12\bar{\zeta}^2 GM}{(1+\zeta\bar{\zeta})^2 c^2}$$

Assuming $\phi = 0, \ \therefore \zeta = \overline{\zeta}$, where $\zeta = e^{i\phi} Cot(\theta/2)$. Transforming the stereographic coordinates to (z, b), we get

$\hat{\psi}_0 = \frac{GMf(z,b)}{c^2 r^3}$ where f (z, b) is given in chapter 3.

APPENDIX B

TAYLOR SERIES EXPANSION OF THE THICK LENS

$$\hat{X} = \begin{pmatrix} g_1 & g_2 \\ \bar{g}_2 & g_1 \end{pmatrix} s_* + \begin{pmatrix} f_1 & f_2 \\ \bar{f}_2 & f_1 \end{pmatrix}$$

$$g_1 = 0.5\{L_1\sqrt{\Delta}(\sinh w - \sin w) + \cosh w + \cos w\}$$

$$g_2 = 0.5\{-L_1\sqrt{\Delta}(\sinh w + \sin w) - \cosh w + \cos w\}$$

$$f_1 = 0.5\{(L_1 - L_2)(\cosh w + \cos w) + (1/\sqrt{\Delta} - L_1 L_2\sqrt{\Delta})\sinh w + (1/\sqrt{\Delta} + \mathrm{L}_1 L_2\sqrt{\Delta})\sin w\}$$

$$f_2 = 0.5\{(L_1 L_2\sqrt{\Delta} - 1/\sqrt{\Delta})\sinh w + (L_2 - L_1)(\cosh w - \cos w) + (\mathrm{L}_2 L_1\sqrt{\Delta} + 1/\sqrt{\Delta})\sin w\}$$

$$\frac{dg_1}{dw_0} = 0.5\{L_1\Delta(\cosh w - \cos w) + \sqrt{\Delta}(\sinh w - \sin w)\}$$

$$\frac{dg_2}{dw_0} = 0.5\{-L_1\Delta(\cosh w + \cos w) - \sqrt{\Delta}(\sinh w + \sin w)\}$$

$$\frac{df_1}{dw_0} = 0.5\{(L_1 - L_2)\sqrt{\Delta}(\sinh w - \sin w) + (1 - L_1 L_2\Delta)\cosh w\}$$

$$\frac{df_2}{dw_0} = 0.5\{(L_1 L_2\Delta - 1)\cosh w + (L_2 - L_1)\sqrt{\Delta}(\sinh w + \sin w) + (L_1 L_2\Delta + 1)\cos w\}$$

$$w = w_0\sqrt{\Delta}$$

$$\mu = \frac{1}{\det\hat{X}}$$

$$\frac{d\mu}{dw_0} = -\frac{1}{(\det\hat{X})^2}\frac{d(\det\hat{X})}{dw_0}$$

$$\frac{d\det\hat{X}}{dw_0} = \frac{d}{dw_0}\{(g_1^2 - g_2^2)s_*^2 + (f_1^2 - f_2^2)\}$$

$$\{2g\frac{dg_1}{dw_0} - 2g_2\frac{dg_2}{dw_0})s_*^2 + (2f_1\frac{dg_1}{dw_0} + 2g_1\frac{df_1}{dw_0} - 2f_2\frac{dg_2}{dw_0} - 2g_2\frac{df_2}{dw_0})s_*$$

$$+(2f_1\frac{df_1}{dw_0} - 2f_2\frac{df_2}{dw_0})$$

$$\det\hat{X} = (g_1 s_* + f_1)^2 - (g_2 s_* + f_2)^2$$

$$\frac{d\det\hat{X}}{dw_0} = \{(2g_1\frac{dg_1}{dw_0} - 2g_2\frac{dg_2}{dw_0})s_*^2 + (2f_1\frac{df_1}{dw_0} - 2f_2\frac{df_2}{dw_0})$$

$$\det\hat{X} = (g_1 s_* + f_1)^2 - (g_2 s_* + f_2)^2$$

$$= (g_1^2 - g_2^2)s_*^2 + 2(g_1 f_1 - g_2 f_2)s_* + (f_1^2 - f_2^2)$$

$$= (-L_1^2\Delta \sinh w \sin w - L_1\sqrt{\Delta}\sin w\cosh w + L_1\sqrt{\Delta}\cos w\sinh w + \cosh w\cos w)s_*^2$$

$$+ \{L_1\sqrt{\Delta}(L_1 - L_2)(\sinh w\cosh w - \sin w\cos w) + (L_1 - L_2)\cosh w\cos w$$

$$- L_1\sqrt{\Delta}(\frac{1}{\sqrt{\Delta}} - L_1L_2\sqrt{\Delta})\sinh w\sin w + (\frac{1}{\sqrt{\Delta}} - L_1L_2\sqrt{\Delta})\sinh w\cosh$$

$$+ L_1\sqrt{\Delta}(\frac{1}{\sqrt{\Delta}} + L_1L_2\sqrt{\Delta})\sinh w\sin w + (\frac{1}{\sqrt{\Delta}} + L_1L_2\sqrt{\Delta})\sin w\cosh w\}s_*$$

$$\{(L_1 - L_2)^2\cosh w\cos w + (L_1 - L_2)(\frac{1}{\sqrt{\Delta}} - L_1L_2\sqrt{\Delta})\sinh w\cos w$$

$$+ (L_1 - L_2)(\frac{1}{\sqrt{\Delta}} + L_1L_2\sqrt{\Delta})\cosh w\sin w + (\frac{1}{\sqrt{\Delta}} - L_1^2L_2^2\Delta)\sinh w\sin w\}$$

where $w = w_0\sqrt{\Delta}$

$$\mu_T = \mu_0 + w_0 Lt_{w_0 \to 0}(\frac{d\mu_T}{dw_0})$$

μ_T = magnification of the thick lens

μ_0 = magnification of the thin lens

$$\det \hat{X} = Lt_{w_0 \to 0}[\{-L_1^2\Delta \frac{\sinh(w_0\sqrt{\Delta})}{w_0\sqrt{\Delta}} \frac{\sin(w_0\sqrt{\Delta})}{w_0\sqrt{\Delta}}(w_0^2\Delta)$$

$$- L_1\sqrt{\Delta} \frac{\sin(w_0\sqrt{\Delta})}{w_0\sqrt{\Delta}} \cosh(w_0\sqrt{\Delta})(w_0\sqrt{\Delta})$$

$$+ L_1\sqrt{\Delta} \cos(w_0\sqrt{\Delta}) \frac{\sinh(w_0\sqrt{\Delta})}{w_0\sqrt{\Delta}}(w_0\sqrt{\Delta}) + 1\} s_*^2$$

$$\{L_1\sqrt{\Delta}(L_1 - L_2)(\frac{\sinh(w_0\sqrt{\Delta})}{w_0\sqrt{\Delta}} \cosh(w_0\sqrt{\Delta}) - \frac{\sin(w_0\sqrt{\Delta})}{w_0\sqrt{\Delta}} \cos(w_0\sqrt{\Delta}))(w_0\sqrt{\Delta})$$

$$+ (L_1 - L_2)\cosh(w_0\sqrt{\Delta})\cos(w_0\sqrt{\Delta}) - (L_1 + L_1^2 L_2\Delta) \frac{\sinh(w_0\sqrt{\Delta})}{w_0\sqrt{\Delta}} \frac{\sin(w_0\sqrt{\Delta})(w_0^2\Delta)}{w_0\sqrt{\Delta}}$$

$$(\frac{1}{\sqrt{\Delta}} - L_1 L_2\sqrt{\Delta}) \frac{\sinh(w_0\sqrt{\Delta})}{w_0\sqrt{\Delta}} \cosh(w_0\sqrt{\Delta})(w_0\sqrt{\Delta}) +$$

$$(L_1 + L_1^2 L_2\Delta) \frac{\sin(w_0\sqrt{\Delta})}{w_0\sqrt{\Delta}} \frac{\sinh(w_0\sqrt{\Delta})}{w_0\sqrt{\Delta}}(w_0^2\Delta)$$

$$(\frac{1}{\sqrt{\Delta}} + L_1 L_2\sqrt{\Delta}) \frac{\sin(w_0\sqrt{\Delta})}{w_0\sqrt{\Delta}} \cosh(w_0\sqrt{\Delta})(w_0\sqrt{\Delta})\} s_*$$

$$\{(L_1 - L_2)^2 \cos(w_0\sqrt{\Delta})\cosh(w_0\sqrt{\Delta})$$

$$+ (L_1 - L_2)(\frac{1}{\sqrt{\Delta}} - L_1 L_2\sqrt{\Delta}) \frac{\sinh(w_0\sqrt{\Delta})}{w_0\sqrt{\Delta}} \cos(w_0\sqrt{\Delta})(w_0\sqrt{\Delta})$$

$$+ (L_1 - L_2)(\frac{1}{\sqrt{\Delta}} + L_1 L_2\sqrt{\Delta}) \frac{\sin(w_0\sqrt{\Delta})}{w_0\sqrt{\Delta}} \cosh(w_0\sqrt{\Delta})(w_0\sqrt{\Delta})$$

$$+ (\frac{1}{\Delta} + L_1 L_2\sqrt{\Delta}) \frac{\sin(w_0\sqrt{\Delta})}{w_0\sqrt{\Delta}} \frac{\sinh(w_0\sqrt{\Delta})}{w_0\sqrt{\Delta}}(w_0^2\Delta)\}]$$

$$Lt_{w_0\to 0}\det\hat{A}=[-L_1^2w_0^2\Delta^2+1]s_*^2+[2L_1^2L_2w_0^2\Delta^2]s_*+[(L_1-L_2)^2-L_1^2L_2^2w_0^2\Delta^2]$$

$$w_0\Delta=\int\Psi_0dz=\int\frac{GM}{c^2}f(z,b)dz$$

$$=\frac{GM}{c^2}\int\frac{3\{1+2(z/b)^2+2(z/b)(1+(z/b)^2)^{1/2}\}dz}{(z^2+b^2)^{3/2}\{1+3(z/b)^2+2(z/b)^4+2(z/b)(1+(z/b)^2)^{3/2}\}}$$

$$=\frac{3GM}{c^2b^3}\int_{-\infty}^{\infty}\frac{3\{1+2(z/b)^2+2(z/b)(1+(z/b)^2)^{1/2}\}dz}{((z/b)^2+1)^{3/2}\{1+3(z/b)^2+2(z/b)^4+2(z/b)(1+(z/b)^2)^{3/2}\}}$$

$$=\frac{3GM}{c^2b^3}\int_{-\infty}^{\infty}\frac{\{1+2(u)^2+2(u)(1+(u)^2)^{1/2}\}bdu}{((u)^2+1)^{3/2}\{1+3(u)^2+2(u)^4+2(u)(1+(u)^2)^{3/2}\}}$$

$$=\frac{3GM}{c^2b^2}(\frac{4}{3})$$

$$=\frac{4GM}{c^2b^2},\ \text{where}\ b\ \text{is the impact parameter}$$

$$=2\frac{R_S}{b^2},\ \text{where}\ R_S\ \text{is the Schwarzschild radius}$$

$$Lt_{w_0\to 0}\det\hat{A}=[-L_1^2(4R_S^2/b^4)+1]s_*^2+[2L_1^2L_2(4R_S^2/b^4)]s_*+[(L_1-L_2)^2-L_1^2L_2^2(4R_S^2/b^4)]$$

Substituting $L_1=L_2=D_L;\ s_*=D_S$

$$Lt_{w_0\to 0}\det\hat{A}=[-D_L^2(4R_S^2/b^4)+1]D_S^2+[2D_L^3(4R_S^2/b^4)]D_S+[-L_1^2L_2^2(4R_S^2/b^4)]$$

$$
\begin{aligned}
Lt_{w_0 \to 0}(\mu_T) &= Lt_{w_0 \to 0}\left(\frac{s_*^2}{\det \hat{X}}\right) \\
&= \frac{D_S^2}{\{D_S^2 - \frac{4R_S^2 D_L^2 D_S^2}{b^4} + \frac{8D_L^3 D_S R_S^4}{b^4} - \frac{4R_S^2 D_L^4}{b^4}\}} \\
&= \frac{D_S^2}{\{D_S^2 - \frac{4R_S^2 D_L^2 (D_S - D_L)^2}{b^4}\}} \\
&= \mu_0
\end{aligned}
$$

APPENDIX C

COSMOLOGICAL DISTANCE DETERMINATION

The proper distance between 2 objects of redshifts z_1 and z_2 is given by

$$D_{prop}(z_1, z_2) = \frac{c}{H_0} \int_{a(z_2)}^{a(z_1)} \{\frac{\Omega_M}{a} + (1 - \Omega_M - \Omega_\Lambda) + a^2 \Omega_\Lambda\}^{-1/2} da$$

……...C.1

In the above expression a is the expansion parameter;

$$a = \frac{1}{1+z} \text{ ……..C.2}$$

$\Omega_M = \frac{8\pi G \rho_0}{3H_0^2}$ is the density parameter and ρ_0 the present value of the

matter density of the Universe;

$\Omega_\Lambda = \frac{\Lambda}{3H_0^2}$ is the parameter that is related to the cosmological constant

and $H_0 = 70 \frac{\text{km}}{\text{s (kpc)}}$ is the Hubble constant, $c = 3x10^5 \frac{\text{km}}{\text{s}}$ is the speed of light.

$\Omega_R + \Omega_\Lambda + \Omega_M = 1$, where Ω_R is the curvature parameter. Since we assume a flat universe, $\Omega_R = 0$, and the current values used by astrophysicists are $\Omega_M = 0.3$, $\Omega_\Lambda = 0.7$. Substituting these values into equation C.1 and using C.2, we get,

$$D_{prop}(z_1, z_2) = \frac{c}{H_0} \int_{z_2}^{z_1} \frac{-dz}{(1+z)^2 \{0.3(1+z) + \frac{0.7}{(1+z)^2}\}^{1/2}} \quad \text{.....C.3}$$

This equation can be used to determine the cosmological distances to the lens and the source when the redshifts of both are known. The above equation is usually used for redshift values larger than 0.5.

BIBLIOGRAPHY

Alcock et al. 1997, astro-ph/ 9702199 v1

Angonin-Willaime, M. C., Vanderriest, C., Courbin, F., Burud, I., Magain, P. & Rigaut, F. 1999, Astron. Astrophys., **347**, 434

Bernardeau, F. 1999, astro-ph/9901117 v1

Bourassa, R. R. & Kantowski, R. 1975, Ap. J., **195**, 13.

Cabanac, R.A., Valls-Gabaud, D., Jaunsen, A. O,, Lidman, C. & Jerjen, H. 2005, A. & A., **436**, L21-L25

Chae, K-H. & Turnshek, D. A. 1999, Ap. J., **514**, 587

Chang, K. & Refsdal, S. 1979, Nature, **282**, 561.

Chwolson, O. 1924, Astr. Nachrichten, **221**, 329.

Einstein, A. 1911, Annalen der Physik, **35**, 898.

Einstein, A. 1915, Sitzungber. Preub. Akad. Wissensch., erster Halbband, p. 831

Einstein, A., 1936, Science, **84**, 506.

Frittelli, S., Newman, E. T. & Silva-Ortigoza, G. 1998, Class. Quantum Grav., **15**, 689.

Frittelli, S. & Newman, E. T. 1999, Phys. Rev. D **59**, 124001

Frittelli, S, Kling, T. P. & Newman, E. T. 2000, Phys. Rev. D, **61**, 064021

Frittelli, S, Kling, T. P. & Newman, E. T. 2000, Phys. Rev. D, **63**, 023006

Hammer, F. 1984, Gravitation, Geometry and Relativistic Physics: Proceedings of the

"Journees relativists", Springer-Verlag, Berlin

Hewitt, J. N., Turner, E. L., Schneider, D. P., Burke, B. F., Langston, G. I. & Lawrence, C.R. 1988, Nature, **333**, 537

Huchra, J. P. 1986, Nature, **323**, 784

Jackson, N.., Xanthopoulos, E. & Browne, I. W. A., 2000, M.N.R.A.S., **311**, 389

Janis, A. I. & Newman, E. T. 1965, J. Math. Phys., **6**, 902

Jaroszynski, M., Park, C., Paczynski, B. & Gott, J. R. 1990, Ap. J., **365**, 22

Kayser & Squires 1993, Ap. J., **404**, 441

Kovner, I. 1987, Ap. J., **316**, 52

Laplace, P. S. 1795, "Exposition du systeme du monde"

Lynds, R. & Petrosian, V. 1986, Bull. Am. Astron. Soc. **18**, 1014.

Mao, C., Solis, D. J., Reiss, B. D., Kottmann, S. T., Sweeney, R. Y. 2004, Science, **303**, Issue 5655, 213

Mellier, Y. 1999, Ann. Rev. Astron. & Astrophy., **37**,

Metcalf, B. & Silk, J. 1998, Ap. J. Lett. **492**: L1

Metcalf, R. B. 2004, astro-ph/0412538

Metcalf, R. B. & Zhao, H. 2002, Ap. J. **567**, L5

Mitchell, J. 1784, Philo. Trans. R. Soc. London, **74**, 35

Moustakas, L.A. & Metcalf R.B. 2005, M.N.R.A.S., **339**, 607

Narayan, R. & Bartelmann, M. 1998, "Lectures on Gravitational Lensing" astro-ph/9606001.

Newton, I. 1704, Optiks

Newman, E.T. & Penrose, R. 1962, J. Math. Phys., **3**, 566

Newman, E. T. & Tod, K. P. 1980, General Relativity and Gravitation, **2**, 1

Paczynski, B. 1986, Ap. J., **304**, 1.

Paczynski, B. 1996, Annu. Rev. Astron. & Astrophys., **34**, 419.

Rattenbury, N.J. et al. 2005, astro-ph/0506013

Refsdal, S. 1964, M.N.R.A.S., **128**, 295.

Refsdal, S. 1964, M.N.R.A.S., **128**, 307.

Refsdal, S. 1966, M.N.R.A.S., **134**, 315.

Refsdal, S. 1966, M.N.R.A.S., **132**, 101.

Rhoads, J., Malhotra, S. & Dell'Antonio, I. 1999,
STScI / WIYN / AURA / NOAO / NSF

Rijkhorst, E.J. 2002, Ph.D. Thesis, University of Leiden

Schneider, P., Ehlers, J. & Falco, E. E. 1992, Gravitational Lenses, Springer, Berlin.

Scranton, R., Menard, B., Richard, G.T., Nichol, R.C., Myers, A.D., Jain, B.,
Gray, A., Bartelmann, M., Brunner, R.J., Connolly, A.J., Gunn, J.E., Seth,
R.K., Bahcall, N.A., Brinkman, J., Loveday, J., Schneider, D.P., Thakar,
A. & York, D. G. 2005, astro-ph/0504510 v1

Soldner, J. 1804, Berliner Astron. Jahrb., p161

Soucail, G., Mellier, Y., Fort, B, Hammer, F. & Mathez, G. & Cailloux, M.
1988, Astr. Ap., **191**, L19

Turnshek, D. E., Turnshek, D. A., Craine, E. R. & Boesjaar, P. C. 1985, An Atlas of
Digital Spectra of Cool Stars (Tucson: Western Research Co.)

Turnshek, D. A., Lupie, O. L., Rao, S. M., Espay, B. R. & Sirola, C. J. 1997,
Ap. J., **485**, 100

Tyson, J. A., Valdes, F. & Wenk, R. A. 1990, Ap. J., **349**, L1.

Udalski, A. et al. 2005, astro-ph/0507265

Virbhadra, K. S. & Ellis, G. F. R. 2000, astro-ph/9904193

Walsh, D., Carswell, R. F. & Weymann, R. J. 1979, Nature, **279**, 381.

Wambgnass J. & Schechter, P. L. 2002, Ap. J., **580**, 685

Xanthopoulos, E., Browne, W. A., King, L. J., Koopmans, L.V.E., Jackson, N. J., Marlow, D. R., Patnaik, A. R., Porcas, R. W. & Wilkinson, P. N. 2004, M.N.R.A.S.

Zwicky, F. 1937, Phys. Rev., **51**, 290.